UNIVERSITY OF CALIFORNIA

Los Angeles

The Nonlinear Dynamics of Coupled Hair Bundles

A dissertation submitted in partial satisfaction of the requirements

for the degree Doctor of Philosophy in Physics

by

Tracy-Ying Zhang

2017

ABSTRACT OF THE DISSERTATION

The Nonlinear Dynamics of Coupled Hair Bundles

by

Tracy-Ying Zhang

Doctor of Philosophy in Physics

University of California, Los Angeles, 2017

Professor Dolores Bozovic, Chair

The sensitivity of the auditory system depends in part on the active response of hair cells in the inner ear. Individual hair bundles display frequency selectivity and compressive nonlinearity in response to stimuli. In many auditory and vestibular end organs, the hair bundles are coupled by overlying structures. This motivates our study on how coupling affects the hair bundle sensitivity. We coupled two to four spontaneously oscillating bundles with a microbead, and applied mechanical stimuli to the group. Under these coupling conditions, innate oscillations synchronized, and oscillations became more regular. Furthermore, the synchronized bundles exhibited broad frequency selectivity, over a bandwidth encompassing each bundle's natural frequency. The amplitude of the response also showed compressive nonlinearity. On the other hand, similar experiments performed on bundles coupled under the otolithic membrane showed

completely linear behavior. Our data suggests that coupling plays a role in the dynamics and sensitivity of a nonlinear system, though the effect depends on the scale of coupling.

The dissertation of Tracy-Ying Zhang is approved.

Jianwei Miao

Peter M. Narins

Giovanni Zocchi

Dolores Bozovic, Committee Chair

University of California

2017

Table of Contents

List of figures

Acknowledgements

1. Chapter 3 is a version of

T. Y. Zhang, S. Ji, D. Bozovic. Synchronization of Spontaneous Active Motility of Hair Cell Bundles. Plos One. 2015.

Dr. Seung Ji contributed to developing a numerical model and writing the published manuscript.

Dr. Dolores Bozovic (PI) contributed to designing the experiments and writing the published manuscript.

2. This work was funded by NSF grant number CMMI-1131842.

Vita

Tracy-Ying Zhang

EDUCATION

M.S. in Physics. University of California, Los Angeles, CA. Dec. 2011.

B.S. in Physics and Mathematics (double degree). University of Washington, Seattle, WA. June 2009.

A.S. in Physics. Highline Community College, Des Moines, WA. June 2006

PUBLICATION

- TY Zhang, Ji S, Bozovic D. *Synchronization of Spontaneous Active Motility of Hair Cell Bundles.* PLOS ONE. Nov. 2015.

CONFERENCE PRESENTATIONS

- *Transferring from Community College to a Four-Year University*. American Physical Society Conference for Undergraduate Women in Physics. Jan. 2017.
- *Synchronized Spontaneous Oscillation of Hair Bundles in Bullfrog Sacculus*. Association for Research in Otolaryngology midwinter meeting. Feb. 2015.
- *Artificial Coupling of Hair Bundles in Bullfrog Sacculus*. Association for Research in Otolaryngology midwinter meeting. Feb. 2014.
- *Prototype Flight for the GAPS Experiment, an Indirect Search for Dark Matter*. American Physical Society April meeting. Apr. 2011.
- *Structure of Multiplexers on Stars*. Mathematical Association of America Joint Mathematics Meeting. Jan. 2008.

Chapter 1. Introduction

1. Hair cells

Hair cells of the inner ear are the mechanical sensors that detect air- and ground-borne vibrations and transduce them into electrical signals. A hair cell consists of a cell soma and an array of columnar structures called the stereovilli, which comprise the hair bundle. The actin-filled stereovilli are arranged in rows of increasing height and are coupled together by tip links [1]. The tips of the hair bundles are connected to an overlying membrane, termed the otolithic membrane in the bullfrog sacculus. An incoming stimulus induces a shearing motion between the overlying membrane and the tissue in which the cells are embedded, deflecting the bundle and thus increasing the tension on the tip links. Mechanically sensitive ion channels that are physically coupled to the tip links open in response and allow the inflow of cations [2].

When stimulated by an incoming signal, the hair bundle oscillates in a viscous fluid environment. An internal active process, which pumps energy to amplify the sound-induced vibrations, has been suggested to overcome viscous dissipation [3]. The active process has been experimentally demonstrated *in vitro* [4]. Under conditions that mimic the natural environment, individual hair bundles can exhibit innate oscillations [5] in the absence of any input. This spontaneous motility has been extensively studied in hair cell bundles of the anuran sacculus and can be explained by two processes [6]. Opening and closing of the mechanically sensitive ion channels lead to bistability in the position of the bundle. In addition, an adaptation mechanism mediated by myosin motors provides a feedback mechanism [1], poising the bundle in the regime of highest sensitivity. Interplay between these two processes leads to a relaxation oscillation. Comparisons to the fluctuation-dissipation theory have proven that the observed spontaneous motility requires an underlying energy-consuming process [7].

2. Coupled system of nonlinear oscillators

In vivo, most hair cell bundles are connected to overlying gelatinous structures. Such is the case in frog sacculus, where hair bundles are coupled to the otolithic membrane. Since this is a recurring scheme, how coupling affects the sensitivity of the system merits investigation.

Theoretical studies explored the effects of connecting a number of nonlinear oscillators. Synchronization of active motility was predicted for systems where the individual oscillators exhibit identical or similar frequencies [8]. Moreover, synchronization led to more regular oscillations [9], as well as enhanced sensitivity and frequency tuning [8].

Different phenomena could be expected in a system that shows a broad dispersion of frequencies among the individual cells. With sufficiently large discrepancies in frequencies of the constituent oscillators, coupling could lead to amplitude death and render the system quiescent [10]. The theoretical model predicting amplitude death is consistent with the observed quiescence of saccular hair bundles, fully coupled by the overlying otolithic membrane [11].

3. Experiment proposal

We wanted to explore coupling in a small system of several hair bundles. The experimental study is motivated by theoretical work on synchronization [8], except that our system also has frequency dispersion. The biological preparation we used was the amphibian sacculus, an organ specializing in detection of low-frequency auditory and vestibular signals [12]. Hair bundles in this preparation showed random distribution of innate oscillation frequency, ranging from a few Hz to 60Hz [13]. Therefore, neighboring hair cells can exhibit quite disparate characteristic frequencies.

We studied how coupling affected the motility of the hair bundles: whether synchronization would occur, or whether the frequency dispersion would actually lead to suppression of oscillations. Also of interest was the role of coupling in mechanical sensitivity. Since theoretical work predicted enhanced sensitivity and frequency tuning, we wanted to examine if this indeed occurred in our system.

Chapter 2. Experimental Procedures

1. Biological preparation

Animal care and euthanasia protocols were approved by the University of California Los Angles Chancellor's Animal Research Committee (protocol number ARC 2006-043-13C), in accordance with federal and state regulations. American bullfrogs (*Rana catesbeiana*) were used for all experiments. Prior to dissection, animals were euthanized while under pentobarbital anesthesia.

We excised the sacculus from inner ear of the bullfrog, and isolated the epithelium containing the hair-cells. The preparation was mounted in a two-compartment chamber, with the basal side exposed to artificial perilymph solution (in mM: 110 Na^+, 2 K^+, 1.5 Ca^{2+}, 113 Cl^-, 3 d-glucose, 1Na^+ pyruvate, 1 creatine, and 5 HEPES), and the apical side exposed to artificial endolymph (in mM: 2 Na^+, 118 K^+, 0.25 Ca^{2+}, 118 Cl^-, 3 d-glucose, and 5 HEPES). This configuration (Figure 1A) simulated the natural cellular environment. The pH value and osmolality of both solutions were kept at 7.3 and 230 mol/kg, respectively. The solutions were oxygenated before use.

For experiments involving coupling hair cells artificially, the otolithic membrane, which naturally coupled all hair cells, first needed to be removed. This was done by first digesting the otolithic membrane with an enzyme (50ug/ml Collagenase), and then gently peeling off the membrane with an eyelash tool.

For experiments investigating natural coupling by the otolithic membrane, dissection and mounting procedures were slightly modified to minimize exposure to calcium. The artificial perilymph solution was replaced with medium-calcium perilymph (250µM Ca^{2+}). This was to prevent weakening of the link between hair bundle and the otolithic membrane. After mounting, the otolithic membrane was left intact.

2. Artificial coupling agent

We used 50μm polystyrene microspheres, which had the right size to couple 3-4 hair bundles. The microspheres were first coated with Concanavalin A, a lectin that binds to the glycoprotein on the hair bundle. The coating process involved mixing microsphere solution (2mg/ml in deionized water) and Concanavalin A solution (2mg/ml in deionized water), at a ratio of 1:3. The mixture was then centrifuged and washed out with endolymph. Since Concanavalin A was toxic to biological issue, the washout was repeated four times. The microspheres were then mixed with endolymph at the concentration of 400μm/ml. We used a pipette to inject 100ul of the microsphere mixture into the endolymph solution on top of the preparation. The microspheres would sink onto the preparation, and in a random distribution on top of the hair bundles (Figure 1B).

The microspheres were readily available, and they bound reliably to spontaneously oscillating hair-bundles. Moreover, their transparency allowed top-down imaging of the hair-bundles underneath. There were, however, several drawbacks. First, because of the curvature, there were more degrees of freedom in the coupling, and the binding could not withstand high amplitude of mechanical stimulus. Lastly, due to the randomness of the deposition method, we could not target specific bundles.

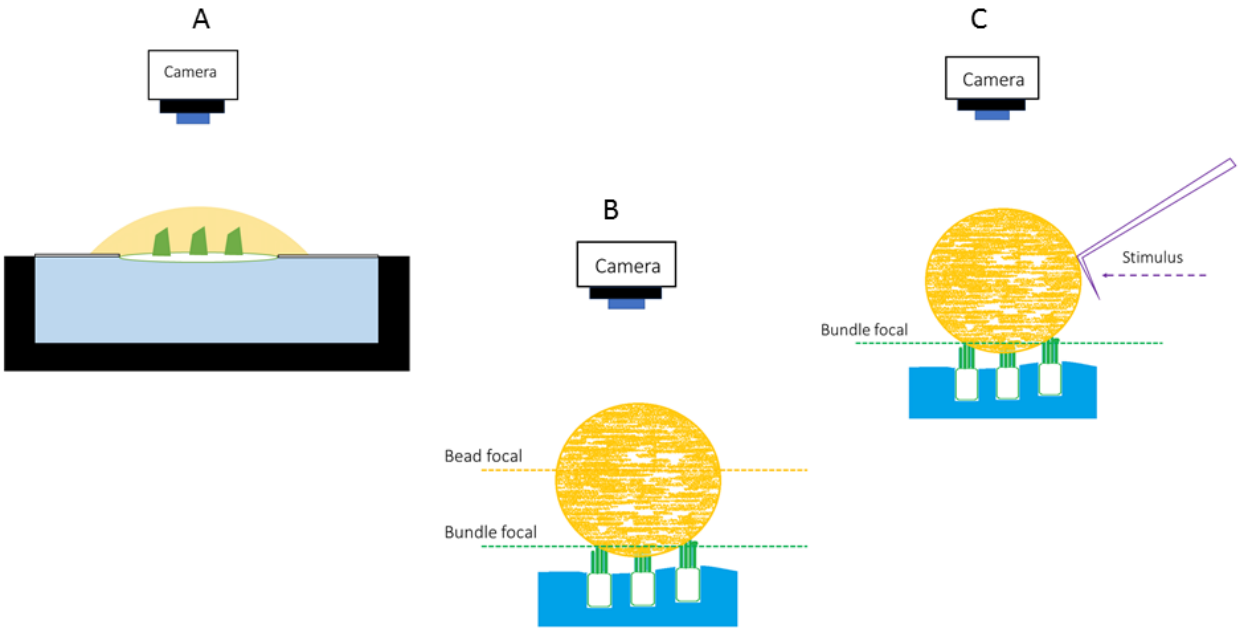

Figure 1. Experimental setup.

(A) Preparation mounted on a two-compartment chapter, with artificial endolymph on top, and artificial perilymph on the bottom. The camera records from a top-down view. **(B)** A polystyrene bead coupling several hair bundles, with attachment via the tip of the stereocilia. **(C)** A glass probe pushing against the equatorial edge of the bead, providing mechanical drive.

3. Mechanical stimulus

Stimulus was provided by a glass probe mounted on a piezoelectric stimulator, driven by waveforms sent from a function generator. The optimal probe stiffness varied depending on the target. To stimulate a single bundle, probe stiffness was selected to be around 100µN/m. For a group of coupled bundles, the stiffness required was 400µN/m. To stimulate the otolithic membrane, a probe of stiffness around 600µN/m were used.

Probes were dipped into a Concanavalin A solution (2mg/ml in deionized water) for 30 seconds before use. To stimulate a coupled group, the probe was pushed against the equatorial edge of

the bead (Figure 1C), providing horizontal stimulus. The underlying hair bundles were deflected by the imposed movement of the bead.

A different protocol was used to stimulate the otolithic membrane. We used a probe with a vertical tip to either push on the side of the otolithic membrane, or to embed it partly into the membrane. For the embedding procedure, we sent a slow sine wave (3Hz) to the probe as it was lowered onto the membrane, and viewed the bundles underneath the membrane. As soon as the probe was sufficiently embedded, the bundles showed a movement in response to the sinusoidal stimulus.

4. Recording Data

Hair bundles were imaged in a top-down configuration with an upright light microscope (Olympus B51W). The image was further magnified and projected onto a Complementary Metal Oxide Semiconductor (CMOS) camera. Two camera models were used: Photron SA-1.1, and a Hamamatsu C-11440.

The choice of camera depended on the trade-off between frame rate, field of view, and recording length. The Photron camera allowed frame rates of 1000 fps, at a magnification of 500x, and a field of view that encompassed up to 20 hair bundles. However, at the maximal field of view, the recording length was limited, The Hamamatsu camera did not have a limit on recording length, but the frame rate depended on the field of view. In order for the field of view to cover a synchronized group of bundles, the maximal frame rate was 500 fps, and the magnification could be no greater than 250x.

Therefore, for recordings of spontaneous oscillations, we used the Photron camera with 500x magnification, and frame rate from 250 to 1000 fps. For recordings of the otolithic membrane,

we used the Photron camera with 250x magnification, and frame rate of 250 fps. For experiments that involved longer recordings, such as chaos in the coupled system and response to stimulus, we used the Hamamatsu camera with 250x magnification and 500 fps.

For artificial coupling, recording was taken at two different focal levels: the tips of the stereociliary bundles, and the equatorial level of the microsphere. The stereociliary tips were visible through the coupling agent. For otolithic membrane experiments, recording was also taken at the focal level of the stereocilia. Bundles were also visible through the otolithic membrane.

Data was stored as a sequence of images, and later processed with a program in Matlab. In order to extract positional information, we analyzed the intensity profile of bundles and found the change from frame to frame. The pixel conversion was 108.9 nm/pixel for 250x magnification, and 54.45 nm/pixel for 500x magnification. Therefore, capturing the change of a few nm would require averaging multiple rows of pixels.

5. Data analysis

5.1 Image analysis

Image sequences were analyzed using programs written in Matlab. In gray-scale, each hair-bundle appeared as a high area of intensity. The position of the hair bundle was defined as the center of the intensity profile. Thus, by tracking the change in the center position, we could characterize the hair bundle's motility. To minimize noise, only parts of the intensity profile greater than a set threshold were included in the calculation. The best threshold level was determined empirically, and varied between the minimum and medium of the intensity.

Even at the highest magnification, the position change from frame to frame was below the size of a single pixel. Therefore, in order to extract the position data, it was necessary to average a dozen rows of pixels. For noisy recordings, we also smoothed the images with a Gaussian filter.

For synchronization analysis, we tracked the motion of individual hair-bundles and the overlying microsphere. The latter was tracked at both the equatorial focal level and the stereocilia focal level. At the equatorial level (Fig 1A), we tracked the edge of the sphere. At the stereocilia level (Fig 1C), we tracked spots (local imperfections in the polystyrene bead) which provided sufficient contrast to be tracked. By averaging the motion of several spots, we extracted the movement of the microsphere.

5.2 Trace processing

The numerical data extracted from the images contain optical noise and sometimes a slow drift, due to the inevitable sagging of a biological preparation. The latter effect was more pronounced in long recordings. To eliminate this drift, we used moving average method with a very large bin (1000 frames) to determine the slow trend, and subtracted it from the trace. This resulted in a signal with zero offset. To remove the noise, we used a lowpass filter (125Hz to 250Hz cutoff), also accomplished with a moving average method.

Chapter 3 Synchronization of Spontaneous Motility

1. Synchronization

1.1 Group Motility

We observed that when coupled by the overlying bead, spontaneous oscillations can synchronize. This was confirmed by tracking the movement of hair bundles through the bead (Figure 2C). Typically, 4 to 6 hair bundles would be positioned underneath the bead. Of those, 3 to 4 hair bundles would be synchronized (Figure 2D). Hair bundles located closer to the center of the bead tended to be synchronized, while those father outside (edge bundles) were less likely to. This is indeed consistent with the spherical geometry of the polystyrene bead.

The collective motility of the synchronized bundles was sufficient to move the overlying bead, giving rise to oscillations up to 80nm in amplitude (Figure 2B). We could track the bead motion in two focal planes: at the equatorial plane of the bead (Figure 2A), or at the stereocilia plane (Figure 2C). In the latter case, the bead was not in focus, but local non-uniformities seen as spots could be readily imaged. By tracking the movement of these spots and averaging them, we could extract the bead motion in the same recordings in which the bundle motion was imaged.

Once the bead was removed, the hair bundles were thus de-coupled (Figure 2E). They were still active, indicating that the coupling process did not cause much damage. As expected for unencumbered bundles, they all exhibited different and uncorrelated oscillations profiles (Figure 2F).

1.2 Correlation

The motion traces of synchronized hair bundles were both phase-locked and in-phase, which became apparent when the traces were overlaid together (Figure 2H). Every cycle of the synchronized bundles, as well as the bead, showed large overlaps. We quantified the degree of synchronization with the cross correlation function. Given time series x(t), and y(t), the cross correlation function f(t) is defined as

$$f(t) = \frac{< x(\tau), y(t+\tau) >}{\sqrt{< x(\tau), x(\tau) >< y(\tau), y(\tau) >}}$$

f(t) is normalized to 1. We used the maximum peak in f(t) to determine the cross correlation coefficient (peak value) as well as the lag (peak location). Two identical traces would therefore have correlation coefficient of 1 and lag of 0.

We computed the cross correlation coefficient between synchronized bundles and the bead, as well as between the connected bundles. The table of coefficient values is shown in Figure 2G. All the values were high, indicating strong correlation. The correlation between any bundle and bead tended to be higher than between bundles. This was due to additional degrees of freedom between bundles. We used the correlation between bundle and bead as the measurement criteria. If the value was greater than 0.5, we characterized the bundle as synchronized. Since the correlation coefficients of all data sets tended to fall into two clusters: from 0.5 to 0.9, or below 0.2, we used 0.5 as a robust threshold for synchronization.

The correlation lag between traces were all between 0 to 2ms, which was within the time resolution of the recording.

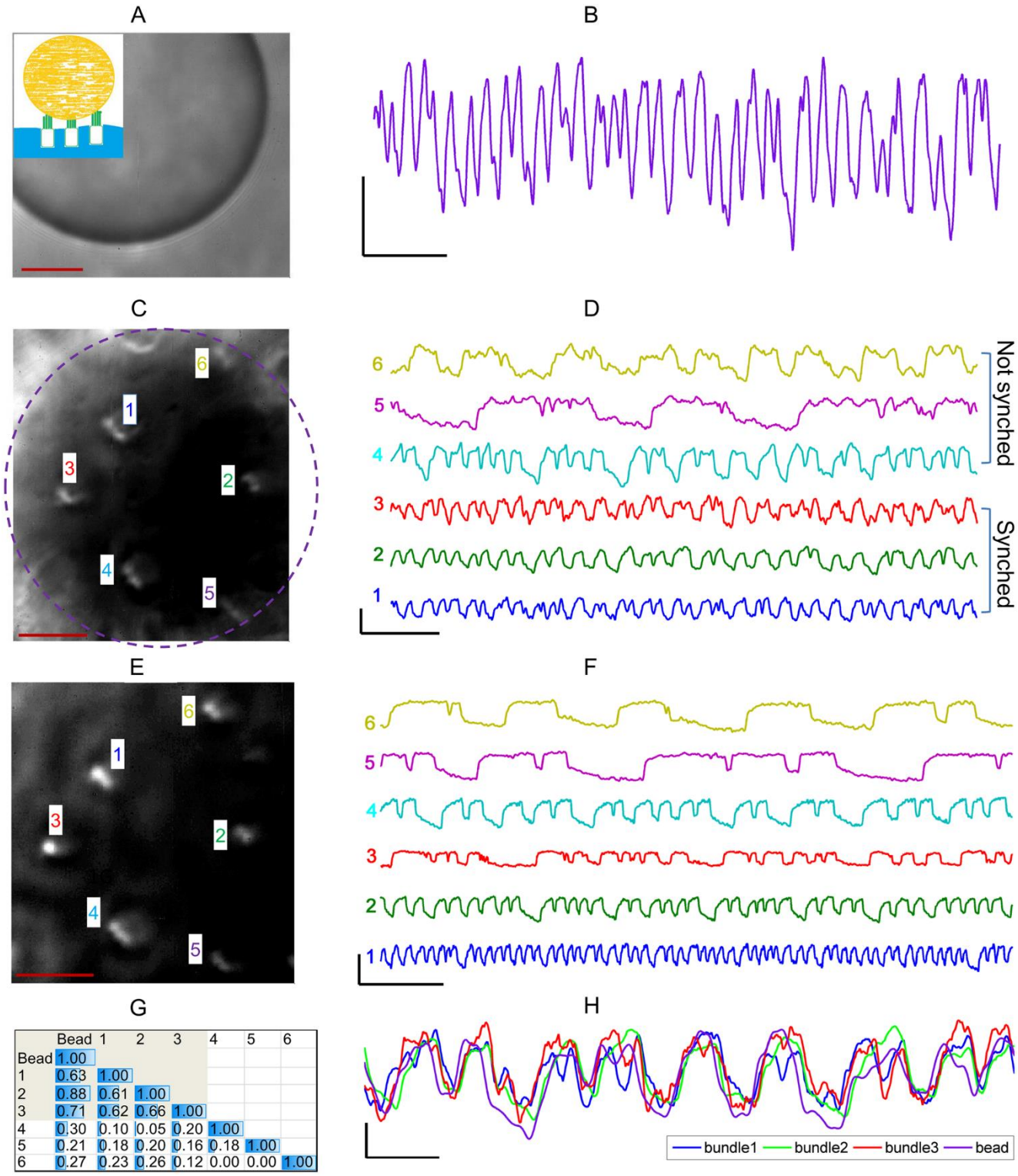

	Bead	1	2	3	4	5	6
Bead	1.00						
1	0.63	1.00					
2	0.88	0.61	1.00				
3	0.71	0.62	0.66	1.00			
4	0.30	0.10	0.05	0.20	1.00		
5	0.21	0.18	0.20	0.16	0.18	1.00	
6	0.27	0.23	0.26	0.12	0.00	0.00	1.00

Figure 2 Synchronization of spontaneous oscillations.

(A) Image of a polystyrene sphere at the equatorial plane of focus, obtained in a top-down view. Scale bar = 10 μm. Inset shows a schematic of the sphere on top of the bundles, in a sideways view. **(B)** Motion trace of the microsphere obtained at the equatorial plane. Scale bar x = 400 ms, y = 40 nm. **(C)** Top-down view of hair bundles, imaged through the overlying polystyrene sphere. Dashed line marks the projection of the rim of the sphere onto this focal plane. Scale bar = 10 μm. **(D)** Traces of spontaneous motion of the hair bundles shown in **C**, denoted by the corresponding numbers. Bundles 1–3 synchronized their motion to each other, whereas those near the rim of the bead (bundles 4–6) did not. Scale bar x = 400 ms, y = 50 nm. **(E)** Top-down view of the hair bundles, obtained after removal of the bead. Scale bar = 10 μm. **(F)** Traces of spontaneous bundle motility, recorded after bead removal. Scale bar x = 400 ms, y = 50 nm. **(G)** Table of the normalized correlation coefficients for the bundle oscillations and those of the bead. Bundles 1–3 were synchronized, and 4–6 were not. **(H)** Overlaid traces of hair bundle (1–3) and bead motility, demonstrating phase-locked oscillation. Scale bar x = 100 ms, y = 20 nm.

2. Frequency Effect

2.1 Oscillation Detection

Adjacent hair bundles on the epithelium typically exhibited different oscillation profiles. Some hair bundles were regular oscillators, with one natural frequency, while others exhibited bursting, with oscillation profiles characterized by bursts of fast oscillations interspersed with intervals of quiescence. Therefore, there was usually a dispersion of natural frequencies present in a synchronized group.

To examine the effect of coupling on oscillation profiles, we needed a standardized measurement of frequency. One method was to take the Fourier transform of the oscillation trace, to compute the power spectrum density (PSD). The peak location of the PSD would be the characteristic frequency. However, we found that the PSD was often noisy, requiring a fitting algorithm to determine the peak location, and in particularly noisy oscillators, the fits were not accurate.

Therefore, we used an oscillation detection algorithm to analyze the oscillation trace. The algorithm detected rapid transitions in the time series, subject to thresholds on both amplitude and slope. Each oscillation would have two rapid transitions, corresponding to the channel opening and channel closing parts of the mechano-transduction cycle. We defined one cycle period, T, as separation between adjacent channel openings (Figure 3A). The cycle frequency was defined as 1/T. From a sufficiently long recording (>5s), we could get a robust histogram of cycle frequencies (Figure 3B). We used kernel density estimation (KDE) to smooth the histogram into a curve, and defined the peak location of the curve as the characteristic frequency of the hair bundle. The shape of the curve also gave information about the regularity of the oscillations, which will be discussed later.

2.2 Frequency convergence

Our results showed that coupling pulled disparate natural frequencies together. Examining the individual hair bundles in a synchronized group, we found that their frequencies had a very small spread when synchronized, compared to the frequency dispersion when de-coupled (Figure 4A). Moreover, the mean group frequency didn't change much between synchronized and de-coupled conditions, suggesting that bundles converged to the group mean frequency.

We also observed dependence of the induced frequency shift on the correlation coefficient between the bundle and the bead (Figure 4B). Within each group of hair bundles, higher correlation coefficients corresponded to smaller ΔFreq, indicating that bundles synchronized more readily when the innate frequencies matched more closely the mean frequency of the group.

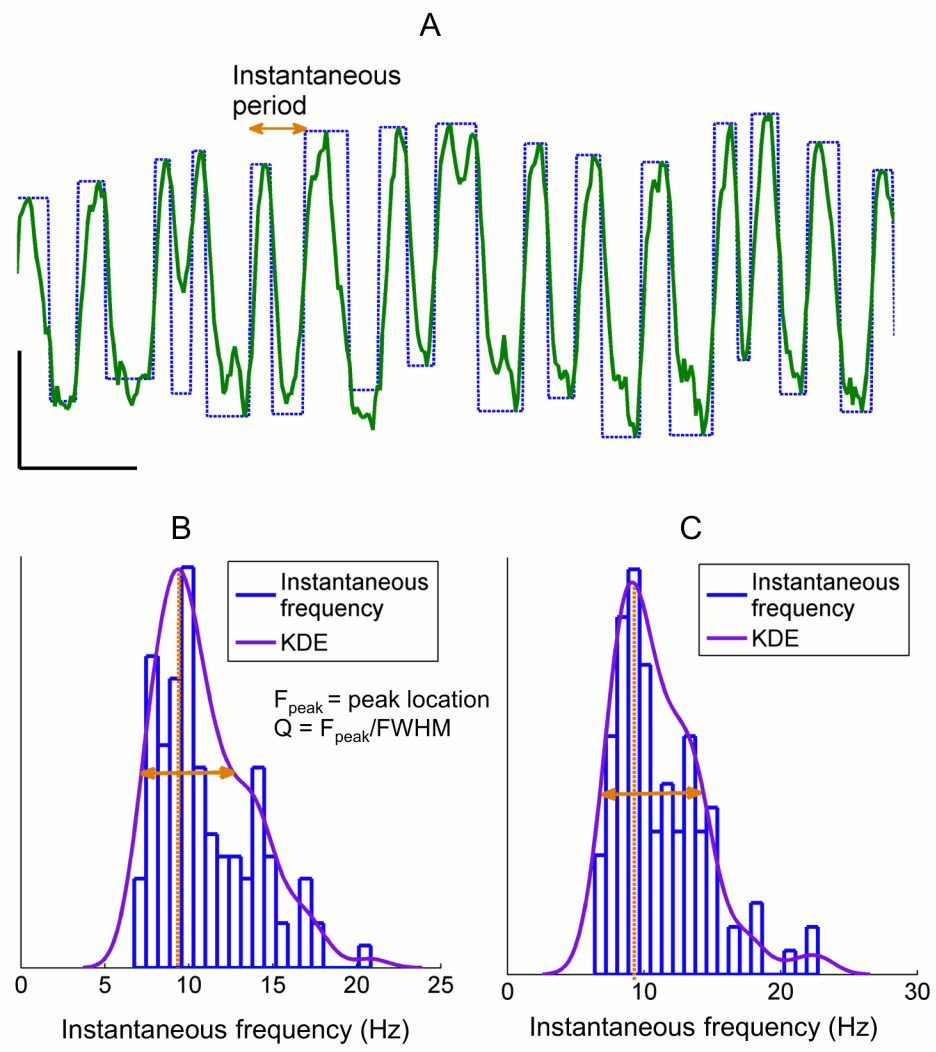

Figure 3. Extracting the frequency and quality factor from the oscillation trace.

(A) A typical recording of the innate motility exhibited by an oscillating hair bundle. The superposed square wave trace represents the rapid positive and negative deflections of the bundle, obtained from the oscillation detection program, described in Methods. The interval between two positive deflections defines the instantaneous period of the cycle. Scale bar x = 200ms, y=20nm. **(B)** Histogram of instantaneous frequencies, obtained from the inverse of the instantaneous period. We used the kernel density estimation (KDE) to smooth the histogram. The peak location of the curve defines the frequency F_{peak}, of the bundle, and the Q-factor is defined as F_{peak}/FWHM. **(C)** Histogram of instantaneous frequencies, with the instantaneous period defined by the interval between two negative deflections. No significant difference was observed between the two methods.

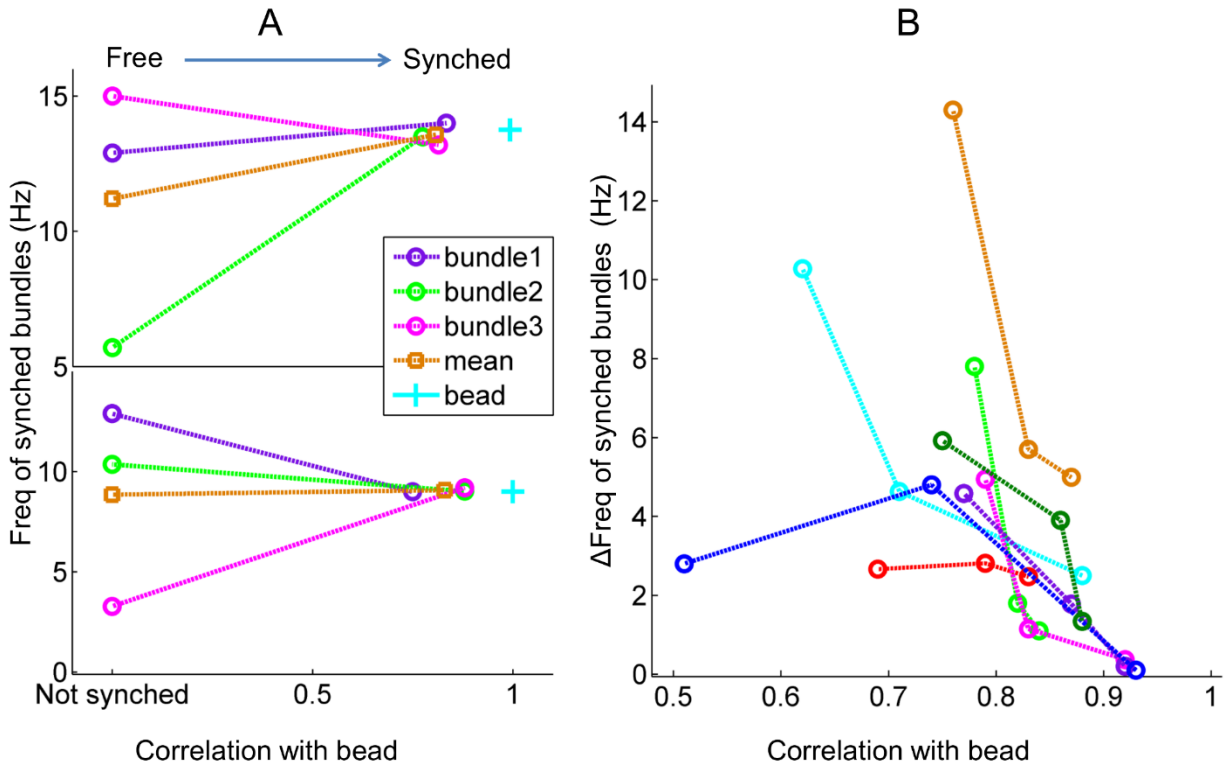

Figure 4. Frequency of the coupled system.

(A) Each panel represents a group of coupled hair cell bundles. For each group, the frequency of bundle oscillations, with and without coupling, is plotted against the correlation coefficient of the bundle motion with respect to the bead. Under coupled conditions, the bundle frequencies converge to the mean frequency of the group. **(B)** Change in the bundle frequency (ΔFreq), defined as the absolute difference between the oscillation frequencies under coupled and uncoupled conditions, versus the correlation coefficient. Each color represents a synchronized group (n=7) of hair bundles. ΔFreq shows a decreasing trend with correlation coefficient.

3. Regularity effect

Synchronized oscillations were observed to be more regular than the noisy innate oscillations of individual hair bundles. To measure the reduction in the variation of the oscillation frequency, we calculated the quality factors of the instantaneous frequency for all spontaneously oscillating hair bundles (n = 6), with and without the presence of an overlying bead (2 examples shown in Figure 5A). Quality factors were found to be consistently higher under coupled conditions,

compared to those extracted from the bundles' innate motility. As a control, the same analysis was performed for the unsynchronized edge bundles (see, for example, bundles 4–6 in Figure 2). Figure 5C shows the quality factors of spontaneous oscillations of edge bundles, with and without the presence of an overlying microsphere. For these groups of cells, quality factors of the individual bundles showed either an increase or a decrease upon the deposition and removal of the bead, with no overall trend, indicating that the regularity of the innate oscillation was not affected.

This measurement was performed for six groups of cells with recordings longer than five seconds. All of the groups showed an improvement in the regularity of spontaneous oscillation (positive ΔQ) as a result of synchronization (Figure 5B). In comparison, the unsynchronized edge bundles showed no trend in ΔQ (Figure 5D). The synchronized system exhibited an enhanced regularity of spontaneous oscillation.

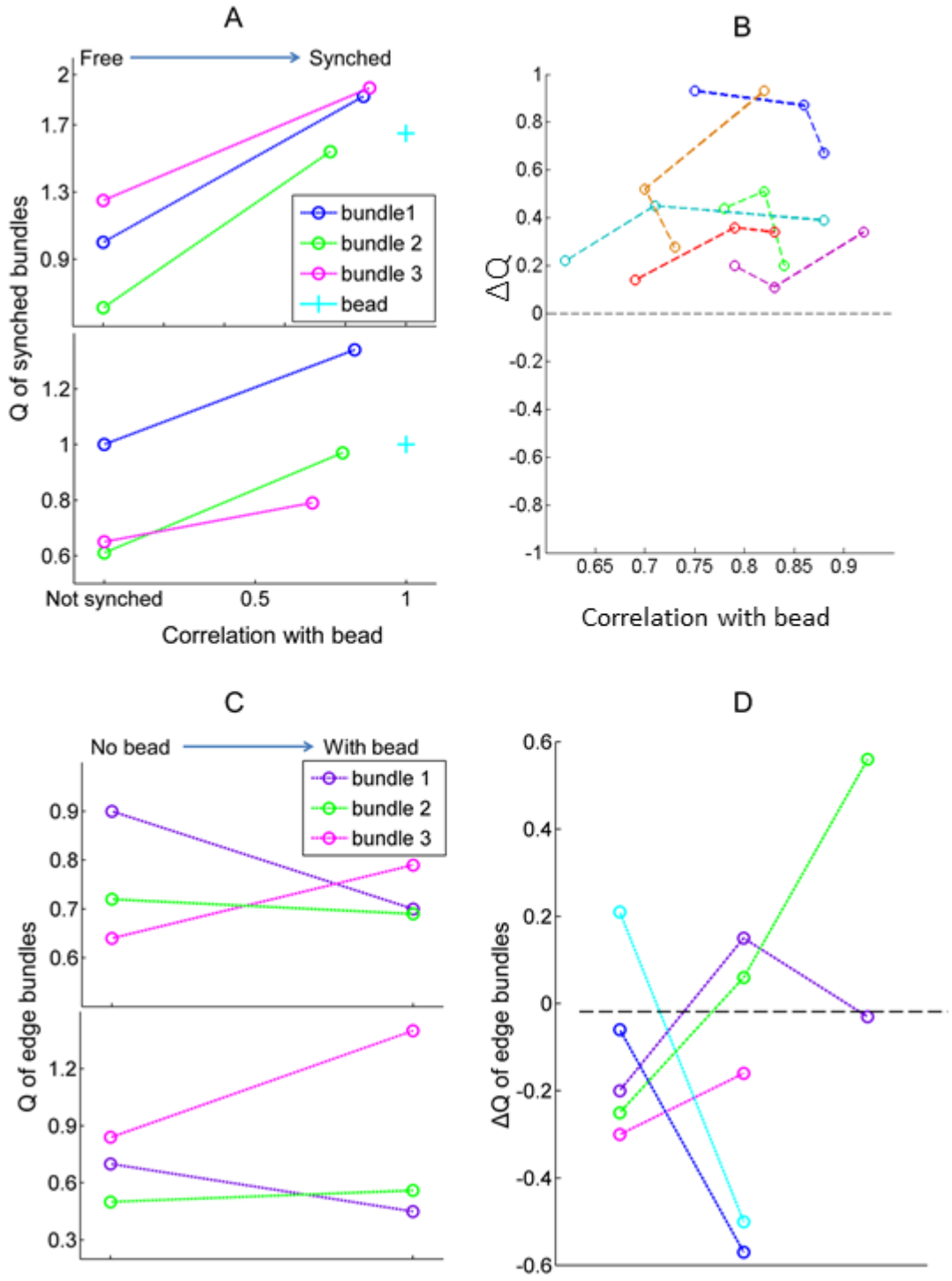

Figure 5. Enhanced regularity of spontaneous oscillations.

(A) Each panel represents a synchronized group of oscillators. For each group, the quality factor of the oscillations exhibited by hair bundles, when synchronized by the bead and upon its removal, is plotted against the bundle's coefficient of correlation with the bead. Synchronization

increases the regularity of the oscillations. **(B)** ΔQ versus the correlation coefficient. ΔQ, defined as $Q_{synchronized}$-$Q_{unsynchronized}$, is measured for each bundle. Each color represents a synchronized group (6 groups total), and each point represents a bundle in the group. ΔQ is always positive, indicating that the synchronized system exhibits an enhanced regularity of oscillation. **(C)** Each panel shows a group of unsynchronized bundles, positioned near the rim of the bead. For each group, we compare the quality factors of the bundles with and without the bead present. The quality factor either increases or decreases, showing no consistent trend. **(D)** ΔQ, obtained for groups of unsynchronized bundles near the rims of the beads. ΔQ was either positive or negative, showing no consistent trends.

4. Multi-mode phase-locking

In addition to the one-to-one mode-locking behavior, we have also observed multimode-locking in synchronized bundles. When this high-order synchronization occurred, the faster bundle's characteristic frequency would be an integer, N, multiple of the slow bundle. When their traces were mapped onto each other, N cycles of the faster bundle would correlate with 1 cycle of the slower bundle (Figure 6AB). We have observed N ranging from 2 to 4. Typically, a synchronized group would have a mix of one-to-one and multimode-locked hair bundles. The correlation coefficient of multimode-locked hair bundle was generally lower than for one-to-one phase-locked bundles.

The mode-locking integer N could be determined by the time evolution of the oscillation phase. We obtained the phase using Hilbert transform. Let y(t) be the oscillation trace. The complex

$$\theta = \arctan\left(\frac{Imag(z)}{Real(z)}\right)$$

form z(t) is defined as z = −*Hilbert*(*y*) + *iy*, where Hilbert(y) is the Hilbert transform of y. The instantaneous phase θ is given by

When we compared the unwrapped phase of the hair bundles, the phase of the faster bundle would grow at a faster rate (Figure 6CD). If we multiplied the unwrapped phase of the slower

bundle by N, then the two phase trends would align. This was confirmed by vector strength test, which showed strong correlation between the faster phase and N times the slower phase.

Multimode phase-locking could arise out of weaker coupling strength. This hypothesis was examined with numerical simulations, which demonstrated the necessary coupling condition for multimode locking to occur (Figure 7 AB).

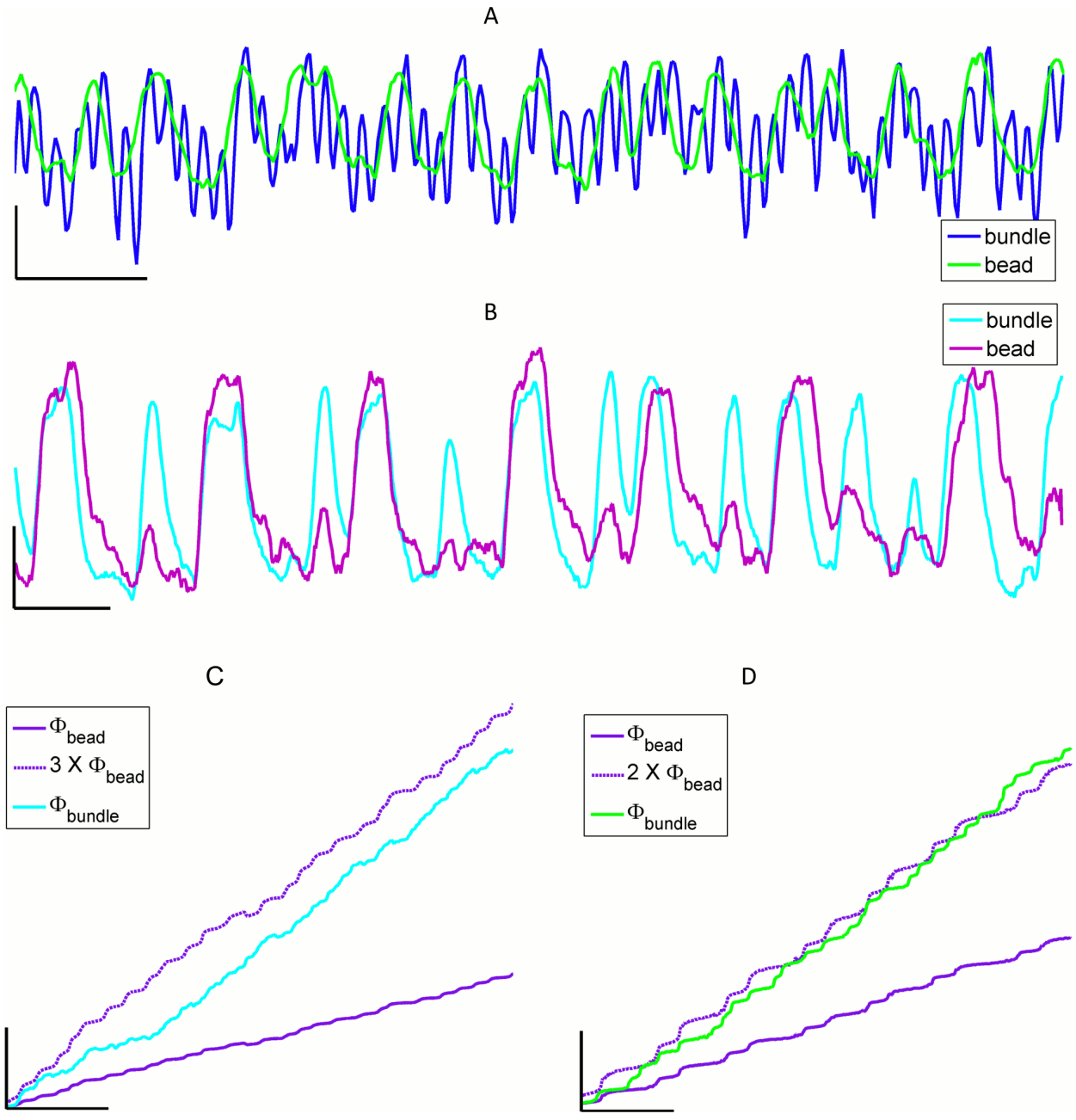

Figure 6. High-order mode-locking.

(A) Traces of motion for a hair bundle and bead pair, showing 3:1 mode locking. Scale bar x = 200 ms, y = 30 nm. **(B)** Traces of motion for a bundle and bead pair, with 2:1 mode locking. Scale bar x = 100 ms, y = 30 nm. **(C)** The unwrapped phase of the pair shown in part A. Instantaneous phase of the bundle (Φ_{bundle}) increases faster than that of the overlying bead (Φ_{bead}). Multiplying Φ_{bead} by 3 leads to a largely parallel evolution of the phases with time. Scale bar x = 300 ms, y = 50 rad. **(D)** The unwrapped phase of the pair shown in part B. Multiplying

Φ_{bead} by 2 leads to a largely parallel evolution of the two phases with time. Scale bar x = 200 ms, y = 20 rad.

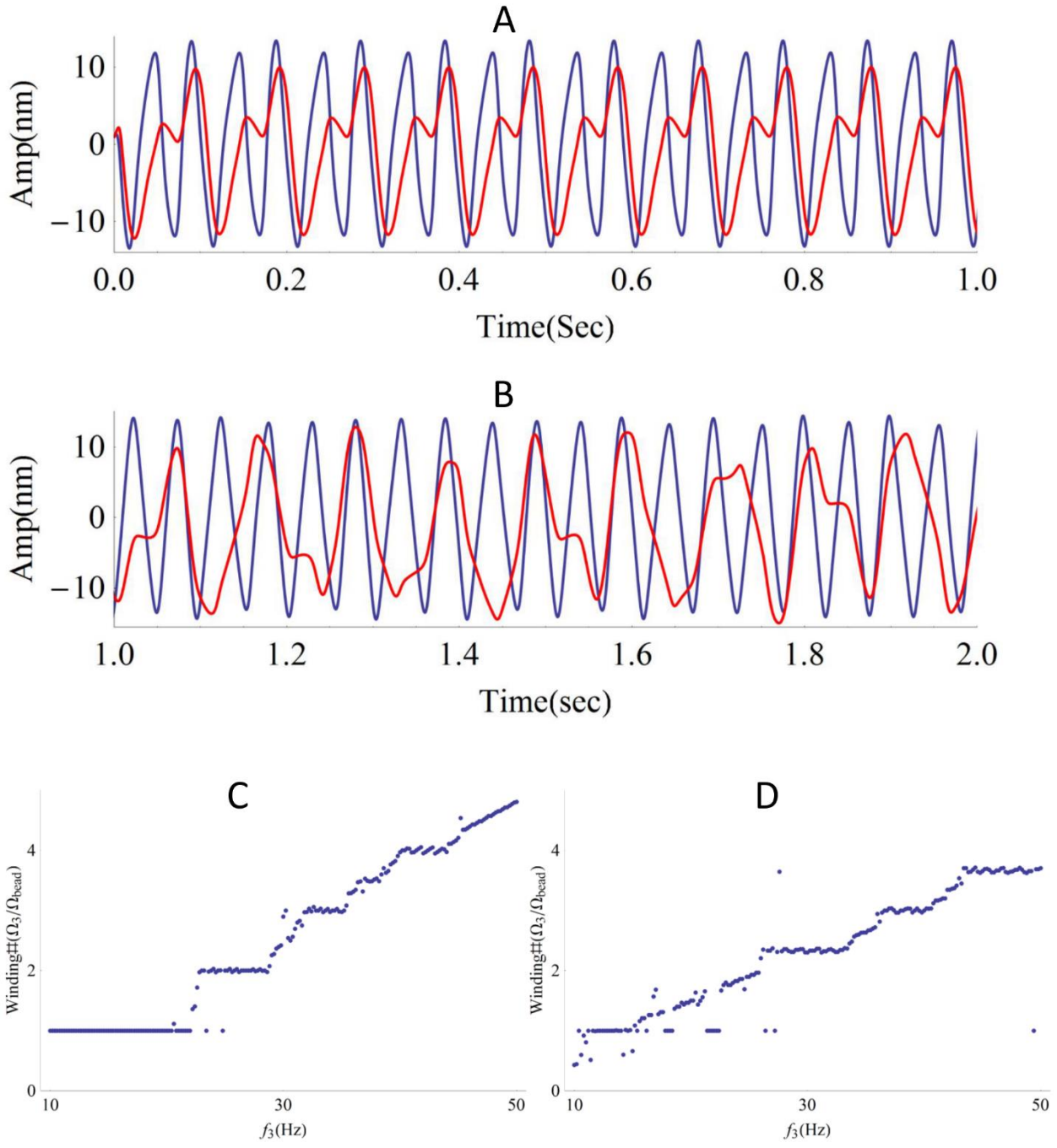

Figure 7. Multi-mode phase-locking by elastic or viscous coupling.

(A) Multi-mode locking due to elastic coupling (Winding Number = 1.98). The red trace shows the bead motion, and the blue trace shows the motion of the hair bundle with the weaker coupling coefficient. The innate frequencies of the three oscillators are Ω_1 = 7Hz, Ω_2 = 17Hz and Ω_3 = 25Hz; the coupling strength is K_1 = 1000 μN /m, K_2 = 1000 μN /m and K_3 = 300 μN /m. **(B)** Multi-mode locking due to viscous coupling (Winding Number = 2.06). The red trace shows the bead motion, and the blue trace shows the motion of the hair bundle with the weaker coupling coefficient. The innate frequencies of the three oscillators are Ω_1 = 7Hz, Ω_2 = 17Hz and Ω_3 = 25 Hz; the coupling strength is ξ_1 = 40 μN*s/m, ξ_2 = 40 μN*s/m and ξ_3 = 2 μN*s/m. Both forms of coupling lead to multi-mode phase-locking. **(C-D)** Winding Number vs. frequency of one of the oscillators. Both forms of coupling show the devil's staircase. **(C)** $K_1 = K_2$ = 1000 μN /m and K_3 = 300 μN /m, Ω_1 = 7 Hz, Ω_3 = 17 Hz. **(D)** $\xi_1 = \xi_2$ = 40 μN*s/m, and ξ_3 = 5 μN *s/m, Ω_1 = 7 Hz, Ω_3 = 17 Hz.

5. Coupling Strength

The coupling between the bead and an underlying bundle can be modeled with viscoelastic elements, as shown in the schematic (Figure 8A).

The viscoelasticity of the hair bundle (hb) is characterized by a stiffness k_{hb} and viscous dragξ_{hb}. Similarly, the connection between the bead and a hair bundle (through concanavalin A) is characterized by k and ξ. With a stimulus imposed on the bead, Δ is the displacement of the bead, and x is the displacement of the bundle. If the stimulus is sinusoidal, we can let $\Delta = \Delta_0 e^{i\omega t}$and $x = x_0 e^{i\omega t+\varphi}$be the response of the bead and bundle, respectively.

The force on the hair bundle is

$$F = m_{hb}\ddot{x} = \xi_{hb}\dot{x} + k_{hb}x + \xi(\dot{x} - \dot{\Delta}) + k(x - \Delta) \quad (1)$$

Since the mass of the hair bundle $m_{hb}$is negligible, the equation of motion is

$$\xi_{hb}\dot{x} + k_{hb}x + \xi(\dot{x} - \dot{\Delta}) + k(x - \Delta) = 0 \quad (2)$$

With sinusoidal stimulus, this becomes

$$\begin{cases} (k_{hb} + k)x_0 \cos\varphi - (\xi_{hb} + \xi)\omega x_0 \sin\varphi = k\Delta_0 \\ (k_{hb} + k)x_0 \sin\varphi + (\xi_{hb} + \xi)\omega x_0 \cos\varphi = \omega\xi\Delta_0 \end{cases} \quad (3)$$

With the substitution

$$A_1 = x_0 \cos\varphi - \Delta_0 \quad A_2 = -\omega x_0 \sin\varphi \quad A_3 = k_{hb} x_0 \cos\varphi - \omega\xi_{hb} x_0 \sin\varphi$$

$$B_1 = x_0 \sin\varphi \quad B_2 = \omega x_0 \cos\varphi - \omega\Delta_0 \quad B_3 = k_{hb} x_0 \sin\varphi + \omega\xi_{hb} x_0 \cos\varphi$$

The solutions are

$$\begin{cases} k = \dfrac{B_3 A_2 - A_3 B_2}{A_1 B_2 - B_1 A_2} \\ \xi = \dfrac{B_3 A_1 - A_3 B_1}{A_2 B_1 - B_2 A_1} \end{cases} \quad (4)$$

Therefore, with a sinusoidal stimulus, we can measure the quantities ω, x_0, Δ_0, φ, and calculate k and ξ.

For this measurement, we sent a stimulus to the bead with a glass capillary probe, which was attached to the equator of the bead. Artificial endolymph was replaced by perilymph, so that the bundles were quiescent. We recorded the motion of individual bundles at the stereocilia focal plane. Spots adjacent to the bundles were also tracked, yielding the motion of the bead.

For the k measurement, the stimulus consisted of a series of sine wave segments, with frequency ranging from 5Hz to 100Hz. For each sine wave segment, we extracted ω, x_0, Δ_0, and φ, which yielded a stiffness value for that frequency. The whole frequency sweep yielded a

distribution (KDE) of stiffness values (Figure 8B). The peak value of the smoothed curve was taken to be k value for this bundle-bead pair, and the width at half maximum gave the error +/- Δk. The results for 8 pairs yielded values from 1.5 (+1, - 0.7) to 4.8 (+/- 1.8) mN/m.

The same procedure was used to measure ξ, in the frequency range 550-650Hz. The results for 4 pair yielded values from 1.9 (+0.16, -0.1) to 3.2 (+/- 1.2) μN*s/m.

The average values for the coupling coefficients are k = 2.5+/-1.1mN/m, and ξ = 2.8+/- 0.7μN*s/m.

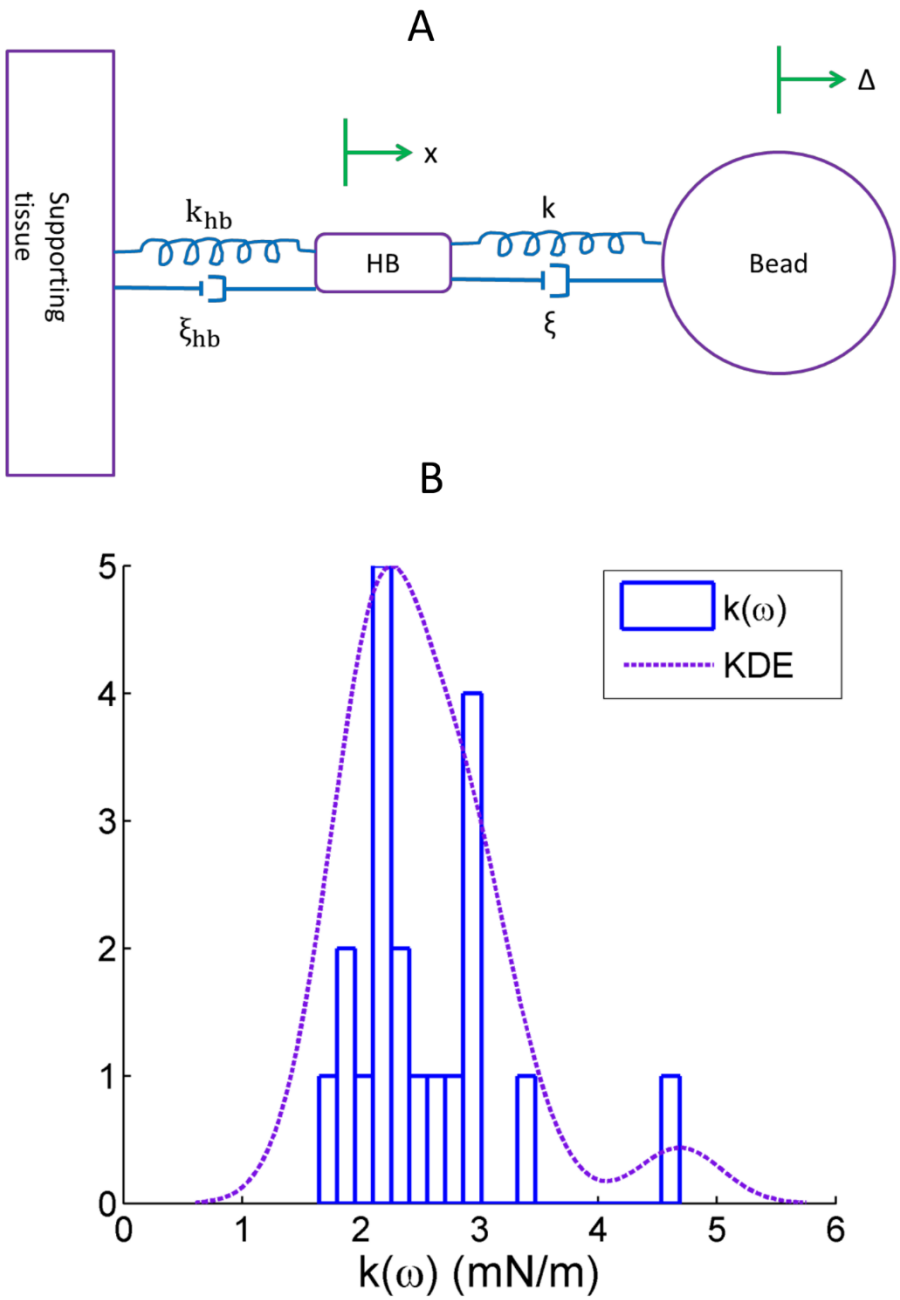

Figure 8. Estimation of coupling strength.

(A) A schematic diagram of the coupling between the bead, the bundle, and the supporting tissue. **(B)** A typical distribution of k(ω) for a single bundle-bead pair. The kernel density estimation curve (KDE) provides a peak value, and the width at half maximum gives the error estimate +/-Δk.

Chapter 4. Mechano-sensitivity of the coupled system

1. Frequency selectivity

1.1 Background

Hair bundles typically exhibit a tuned response to external stimuli. Prior work [14] [15] demonstrated frequency selectivity in hair bundles, with sensitivity peaking at the bundle's characteristic frequency. The shape of the tuning curve depended on the stimulus amplitude, with weaker stimulus producing sharper peaks.

Theory on coupled system predicted enhanced mechanical sensitivity [8], provided that the coupled oscillators were close to identical. Since the amphibian sacculus exhibits frequency dispersion, we wanted to examine the response characteristics of a coupled system of hair bundles that exhibit a spread of natural frequencies.

1.2 Protocol for experiments and data analysis

We applied a mechanical stimulus to the coupled system by attaching a glass probe to the overlying bead. The probe had a stiffness of ~400μN/m. The stimulus consisted of a discrete frequency sweep (Figure 9A), applied at a constant amplitude. The sine wave segments ranged from 1Hz to 40Hz, with 10 cycles per segment. There was a 0.5ms interval between the segments, plus a longer, 2s interval at the beginning and end of the stimulus. The longer intervals were used to confirm that hair bundles remained synchronized during the recording. Only datasets with consistent synchronization during these intervals were considered in the analysis.

The bundle response to each stimulus wave segment was fitted to a sine wave (Figure 9B-D). Amplitude and phase were fitting parameters, while frequency was fixed to the stimulus frequency. The resulting fit provided the phase-locked amplitude. If there was any frequency selectivity, then phase-locked amplitude as a function of stimulus frequency would show a peak. Meanwhile, the degree of entrainment could be measured by R^2 value from the fit statistics. R^2 ranged from 0 to 1, and 1 would mean perfect entrainment to the stimulus.

1.3 Results

We found that synchronized hair bundles exhibited frequency selectivity, despite dispersion in their innate frequencies. The phase-locked amplitude as a function of stimulus frequency (Figure 10A) showed a broad peak, which encompassed both the natural frequency of the individual hair bundles, as well as their synchronized frequency. Every hair bundle within the synchronized group showed frequency selectivity, although the profiles of their tuned response were not the same. Moreover, hair bundles with natural oscillations that were bi-modal (bursting cells), showed frequency selectivity curves with two peaks, such as the bundle 2 in Figure 10A. The broad tuning was observed in all of our datasets (n = 6). The Q-factor of the tuning curve ranged from 0.3 to 1.5 (Figure 10C).

We also examined entrainment as a function of stimulus frequency (Figure 10B). Entrainment was higher than 0.5 for most of the stimulus duration, peaking in the same manner as the phase-locked amplitude. When entrainment was strong, hair bundle response was correlated with stimulus over each cycle sent (Figure 9C). As the stimulus frequency moved away from resonance frequency, entrainment became weaker, and hair bundles began to show phase slips (Figure 9 BD).

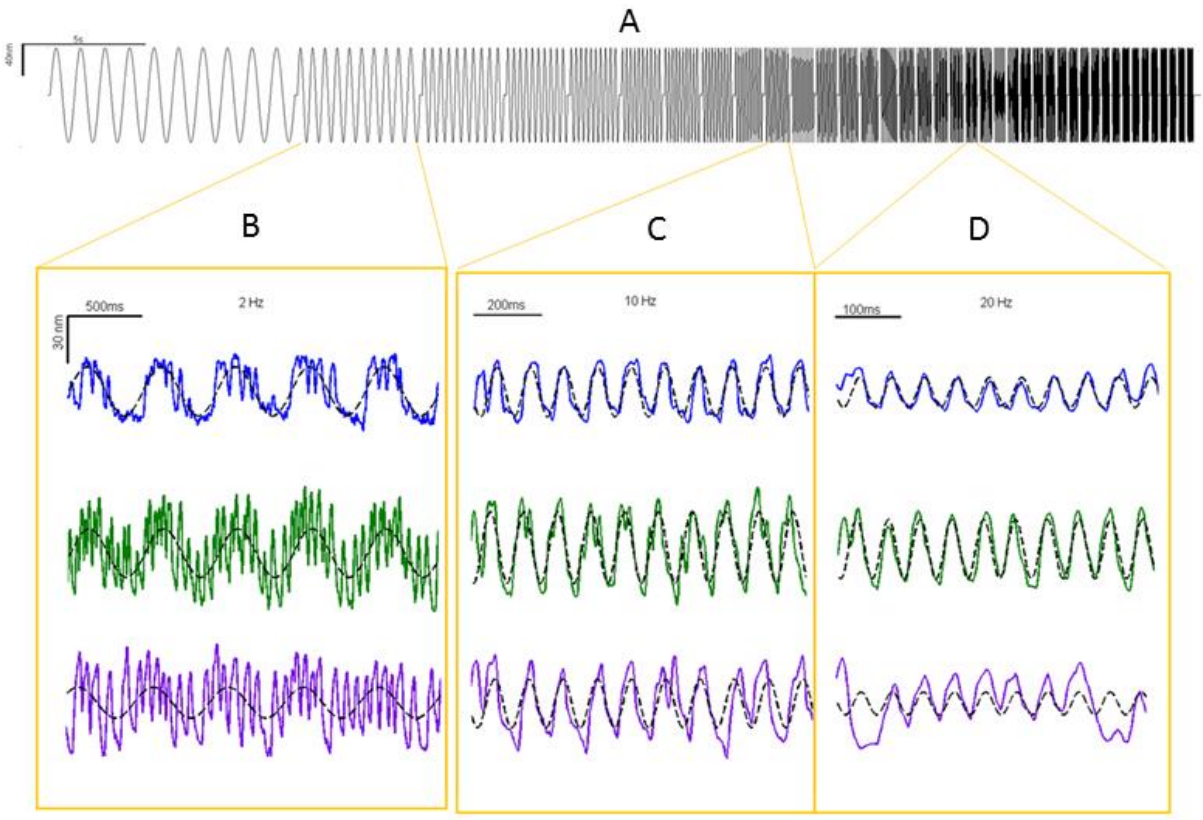

Figure 9. Discrete frequency sweep.

(A) Discrete frequency sweep stimulus waveform. **(B)** Bundle response to 2Hz segment of the stimulus. Each color represents a synchronized bundle, while the dashed black lines represents the sine wave fit. **(C)** Bundle response to 10 Hz stimulus segment. **(D)** Bundle response to 20Hz stimulus segment.

1.4 Comparison with single bundle tuning

Prior measurements had shown that the frequency selectivity of an individual hair bundle depends on the forcing amplitude, with smaller stimuli producing sharper peaks [14]. A direct comparison of the sharpness of frequency selectivity for the coupled bundles and individual ones could not be made, as we did not have an independent measurement of the stimulus force acting on each hair bundles connected to the bead. However, we could make some observations on the differences between synchronized bundles and freely oscillating bundles.

First, the frequency selectivity of an individual bundle always peaked at its characteristic frequency, whereas that was not the case for synchronized bundles, since the frequency of other bundles under the bead also played a role. Secondly, a larger stimulus amplitude was required to invoke entrainment in the synchronized group. Amplitudes below 20nm provided poor entrainment.

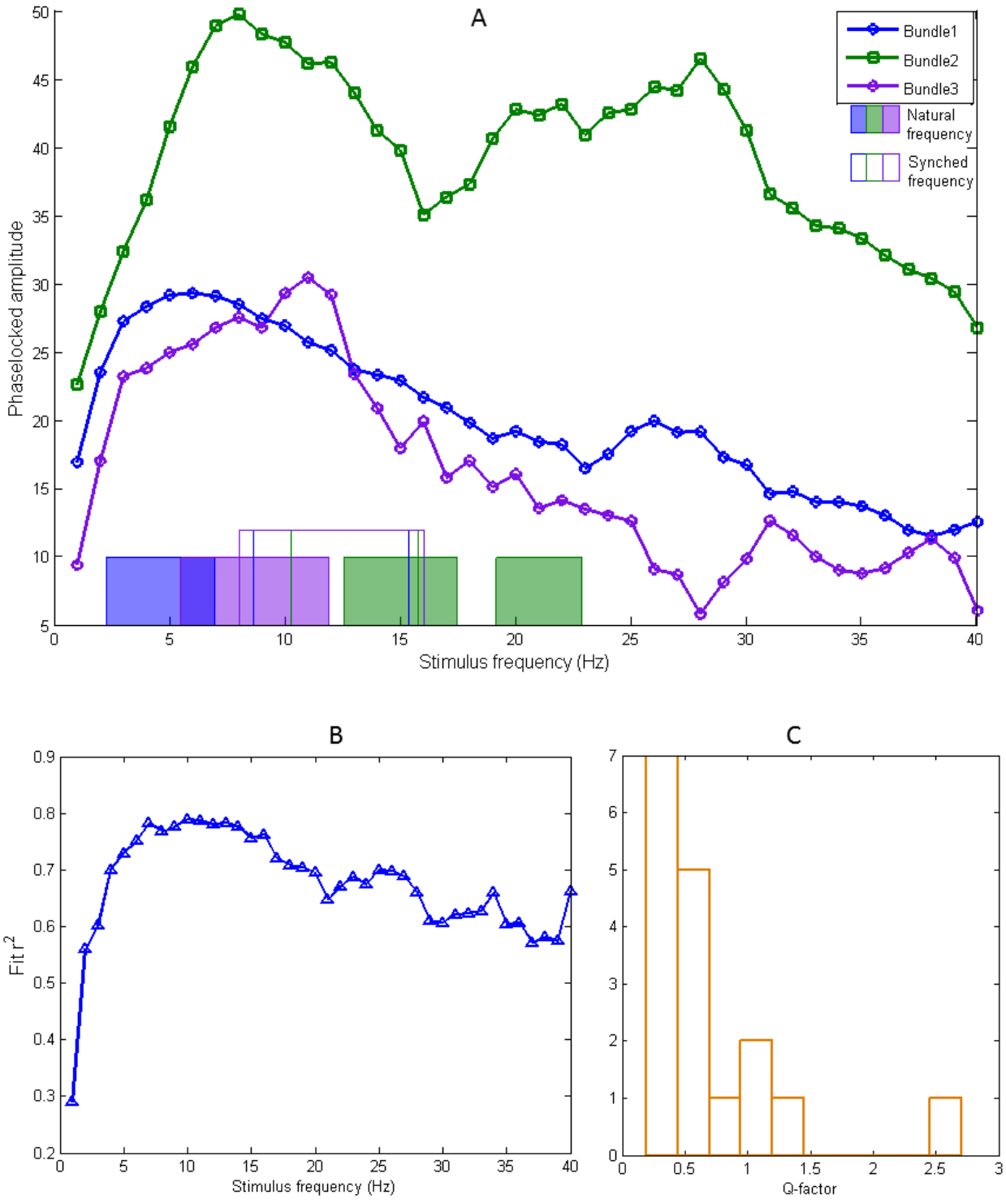

Figure 10. Frequency selectivity of synchronized bundles.

(A) Phaselocked amplitude versus stimulus frequency. Each colored line represents one synchronized bundle. The solid colored boxes represent the characteristic frequencies of the individual bundles (measured under de-coupled condition). The width of the box represents the FWHM of the oscillation frequency. Hollow colored boxes represent the synchronized frequency**.** **(B)** Entrainment of bundle 1 as a function of stimulus frequency. **(C)** Q factor distribution of frequency selectivity curve for synchronized bundles, collected from 6 datasets.

2. Compressive nonlinearity

2.1 Background

Hearing exhibits a remarkably wide dynamical range. For example, in humans, it can encompass 120 dB of signal amplitudes. Compressive nonlinearity throughout the auditory pathway is key to sustaining this feature. On the hair-cell level, compressive nonlinearity also manifests itself in the hair bundle's response to mechanical stimuli. Work by [7] demonstrated this behavior. When the hair bundle was subject to increasing stimulus amplitudes, applied near its natural frequency, there was a region of stimulus amplitude where the bundle response was nonlinear. This feature disappeared when stimulus frequency moved far away from resonance.

Since the nonlinear response was frequency dependent, it could be affected by the frequency dispersion of the synchronized system. We wanted to test if nonlinearity was indeed retained by the coupled system, and whether the effect was different from the single hair bundle.

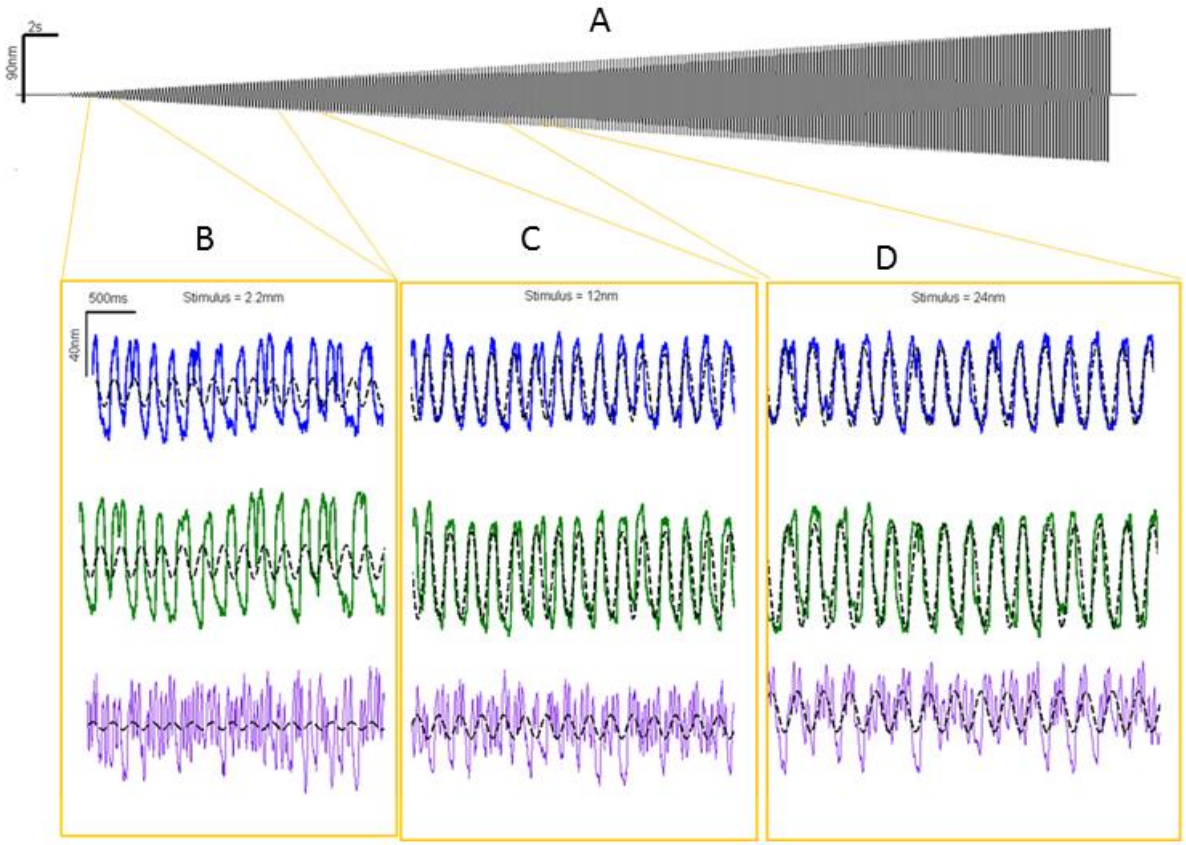

Figure 11. Amplitude ramp sine stimulus.

(A) Sine stimulus with ramping amplitude, from 0nm to 90nm. **(B)** Bundle response in a time window. The width of the window is 15 sinewave cycles, and the mean stimulus amplitude in the window is 2.2nm. Each color represents a synchronized bundle, while the dashed black lines represents the sine wave fit. **(C)** Bundle response in a time window, with mean stimulus amplitude = 12nm. **(D)** Bundle response in a time window, with mean stimulus amplitude = 24nm.

2.2 Experiment and data analysis protocol

We used a probe to apply stimuli to the bead, which would move in response, together with the synchronized bundles. The probe stiffness was 400μN/m. The stimulus consisted of a sine wave at a fixed frequency, with a linearly ramped amplitude (Figure 11A). Over the course of one minute, the sine wave amplitude increased from 0nm to 90nm. There were 2 second intervals of

no drive, at the beginning and end of the stimulus train, which were used to measure spontaneous synchronization. Only datasets with consistent synchronization during these intervals were considered.

To examine the changes in the response amplitude, we divided the stimulus train into moving time windows. Each window spanned 15 cycles of the sine wave, and each subsequent window was moved forward by one cycle. Thus, the windows had significant overlap. Since the stimulus amplitude was linearly increasing, we used the mean amplitude in the window to be the window amplitude (Figure 11 B-D).

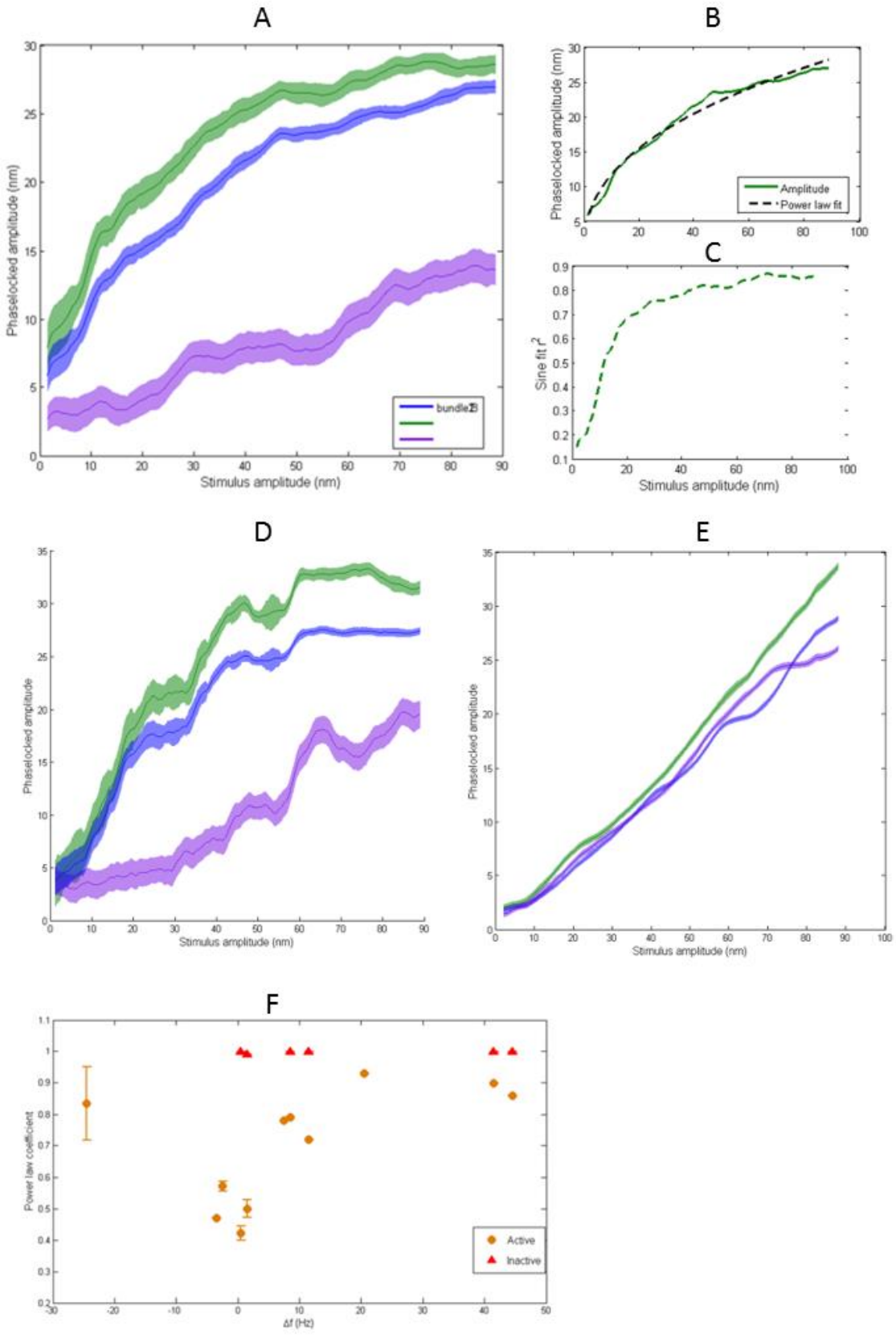
A
B
C
D
E
F
Phaselocked amplitude (nm)
Stimulus amplitude (nm)
Amplitude
Power law fit
Sine fit r²
Phaselocked amplitude
Power law coefficient
Δf (Hz)
Active
Inactive

Figure 12. Compressive nonlinearity of synchronized bundles.

(A) Phaselocked amplitude as a function of stimulus amplitude. Stimulus frequency = 5Hz (on resonance). Each colored line represents a synchronized bundle, while the shaded region represents the error bar. **(B)** Fitting amplitude growth to a power-law. Data taken from bundle 1 in (A). **(C)** Entrainment as a function of stimulus amplitude. Data taken from bundle 1 in (A). **(D)** Phaselocked amplitude as a function of stimulus amplitude, where stimulus frequency = 9Hz (off resonance). **(E)** Phaselocked amplitude versus stimulus amplitude. Stimulus frequency = 5Hz, and the hair cells are inactive. **(F)** Power-law coefficient as a function of Δf (defined as stimulus frequency minus resonance frequency). Yellow dots are data taken from 5 synchronized groups, with active cells. Red triangles are data from control experiments, with synchronized inactive cells.

We also performed control experiments, where 50μM gentamicin was infused into the endolymph bath. Gentamicin blocks the transduction channels in the stereocilia, effectively halting the active process. In the presence of gentamicin, hair bundles did not oscillate. We applied the same mechanical stimulus to synchronized, inactive bundles, and recorded the response amplitudes.

2.3. Results

When subject to on-resonance stimuli, synchronized bundles displayed a compressive nonlinearity (Figure 12A). Entrainment was observed already at stimulus amplitudes of 2nm, and bundle response remained nonlinear until the maximal stimulus amplitudes probed (90nm). Entrainment was stronger for one-to-one mode-locked bundles than for multimode-locked bundles. This likely reflected the fact that the same stimulus was off-resonance for the bundles that displayed high-order mode-locking. Typically, entrainment grew rapidly below 20nm stimulus amplitude, and then gradually approached 1 (Figure 12C). When stimulus occurred a few Hz off-resonance, bundle responses were still nonlinear (Figure 12D).

The nonlinear trend could be fitted with a power law. For on-resonance stimulus, the power law coefficient was about 0.3 (Figure 12B). As stimulus moved off-resonance, the power-law also changed to become more linear, and the coefficient gradually approached 1 (Figure 12F).

In comparison, synchronized hair bundles in control experiments displayed completely linear response to on-resonance stimuli. This indicated that nonlinearity was a product of the active process, and not a passive effect. When we fitted the response curve to a power law, the coefficient was always 1, whether stimulus was on resonance or off-resonance (Figure 12F).

2.4. Comparison to single hair bundles

The synchronized bundles behaved similarly to single bundles in a number of ways. First, with on-resonance stimulus, entrainment could be invoked by very small stimulus amplitudes (about 2nm). Secondly, phase-locked amplitude growth displayed compressive nonlinearity, which was most prominent in on-resonance stimulus, and less so off-resonance. Lastly, the power law coefficient for on-resonance stimulus was 0.3, which was similar to the value obtained in [7].

Our experiments could not probe the high amplitude regime, where nonlinearity typically disappeared above 150nm stimulus amplitude for individual hair bundles. The experimental limitation was due to the coupling between the bead and bundles, which could be compromised by strong forcing of the bead.

Chapter 5. Coupling by the Otolithic Membrane

1. Motivation

Hair bundles in the bullfrog sacculus are naturally coupled by the otolithic membrane, a mass of extracellular tissue that provides both coupling and loading. The membrane is about 25-30μm thick, and it is attached to the epithelium by a network of filaments [16]. The membrane couples around 2500 hair bundles (Figure 13A). Prior work showed that a patch of membrane is of comparable stiffness to the hair bundle [17]. The membrane was shown to provide strong coupling, leading to a coherent response across significant portions of the sacculus [11]. Individual hair bundles are embedded in a fluid sac on the underside of the otolithic membrane, and attached to the wall of the sac.

When naturally coupled by the otolithic membrane, hair bundles do not spontaneously oscillate. Nevertheless, it is an active system [18], and we are interested in how the active process is manifested in terms of the mechanical response. Prior worked showed very broad frequency tuning [18]. We build upon this work to further explore the nonlinearity of the otolithic membrane system. We also want to compare the result to the coupled system of 3 to 4 bundles (via the microsphere).

2. Method

2.1 Biological preparation

The dissection protocol was altered so that the preparation was immersed in NMDG-based saline solution, to avoid exposure to high calcium concentration that characterizes ordinary perilymph. Based on empirical evidence, calcium ions tended to weaken the fiber connection

between the otolithic membrane and the apical surface of the epithelium. Therefore, we avoided exposing the sacculus to high calcium during the dissection process.

We pulled away the otoconial mass from the top of the otolithic membrane, which was otherwise left undisturbed. The preparation was mounted in a two-compartment chamber, with perilymph on the bottom, and endolymph on top, following previously established procedures.

2.2 Mechanical stimulus

A stiff glass probe (~600µm/N) was used to provide mechanical stimulus to the otolithic membrane. Two protocols were used to attach the probe to the membrane, approaching it either from the side edge, or from the top. The edge attachment involved pushing a vertical probe tip against the edge of the membrane, providing a horizontal stimulus. The top attachment involved lowering a slightly slanted probe tip (30 degrees from vertical) to the top of the membrane, and embedding it in the tissue (Figure 13B). Empirical evidence suggested that the embedding method provided more long-range stimulus, affecting hair bundles located farther away from the probe tip. Therefore, we chose this method for most of the measurements.

To ensure best attachment, we sent a 3Hz sinewave through the probe while lowering it gradually with a micro-manipulator. The camera was focused on the stereocilia level below the membrane. As soon as bundles began visibly moving with the sine stimulus, the probe was assumed to have reached optimal position.

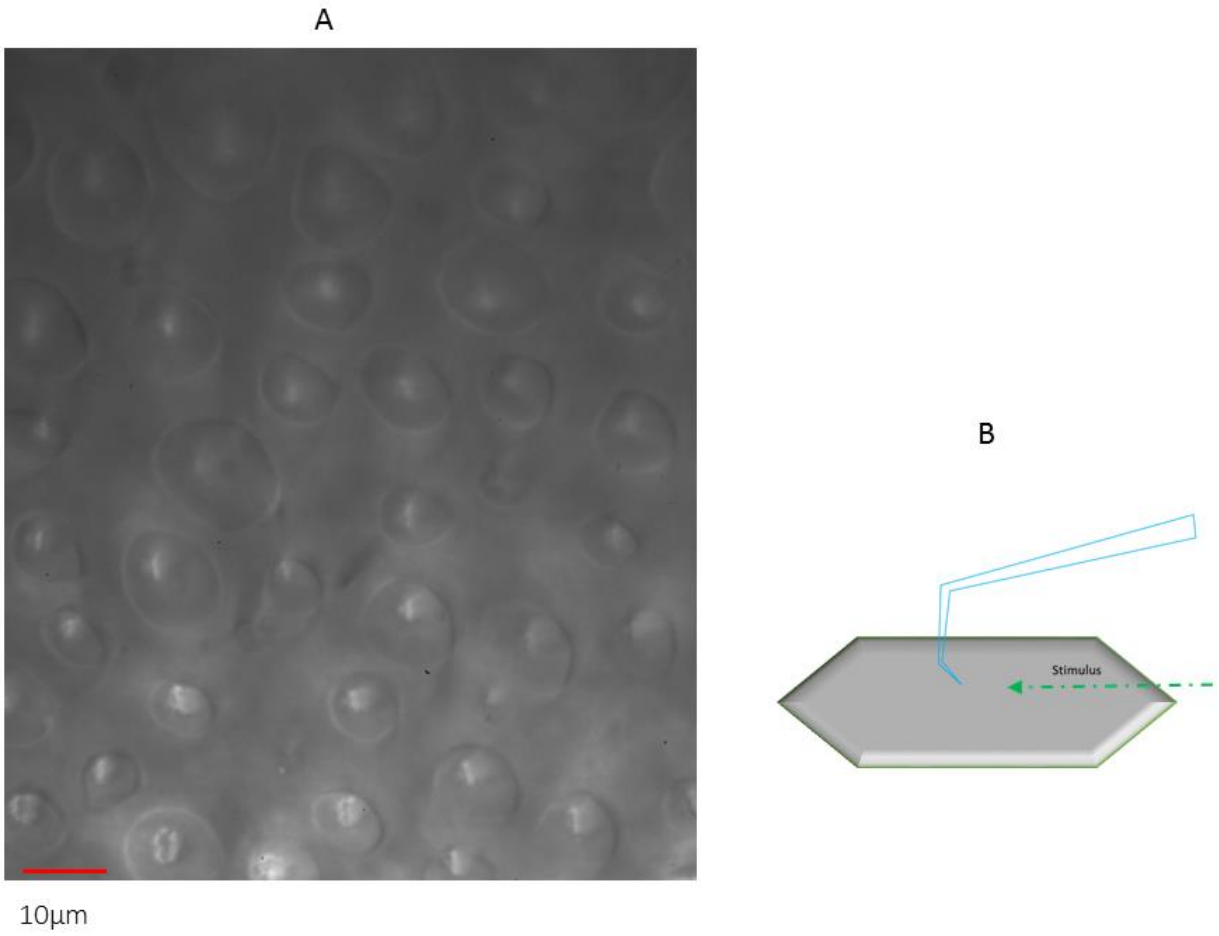

Figure 13. Otolithic membrane experiment.

(A) Top down view of the otolithic membrane and the hair bundles underneath. **(B)** Method of attaching probe to the top of the membrane and sending a horizontal stimulus.

2.3 Control experiment

Any mechanical sensing property measure should reflect the hair bundle's active process. To separate these effect from the passive properties of the structure, we performed control experiments with gentamicin. In these experiments, gentamicin solution was added to the endolymph bath surrounding the hair bundles. Gentamicin is an aminoglycoside which interferes with mechano-transduction channels. At 50µM concentration, it completely stops hair bundle

oscillations, indicating the cessation of the active process. This is effect is reversible, as oscillations return after a wash-out with regular endolymph.

After all measurements were complete, we peeled off the otolithic membrane with an eyelash tool, and observed the state of the hair bundles. If there were 70% or more hair bundles spontaneously oscillating, we considered that to be a verification that the hair bundles were active underneath the otolithic membrane during the experiment.

3. Frequency selectivity

Since the smaller coupled system exhibited frequency selectivity, we wanted to test if this property is retained in a large coupled array. Prior work [18] showed some hints of tuning, but it was very broad. We tested for frequency selectivity with a discrete frequency sweep stimulus, consisting of sine waves of frequencies from 1Hz to 40Hz (Figure 14A), which covers most of the hair bundles' natural frequencies. The frequency segments were ordered randomly, and there were 25 cycles per segment. We measured the response of bundles at various distances from the probe location.

Hair bundles within 50μm from the probe tip showed movement driven by the stimulus (Fig 15B). Farther away, the amplitude of the response dropped off precipitously. We measured the phase-locked amplitude of the bundle response, determined by fitting the evoked movement to a sine wave of the stimulus frequency. Amplitude and phase were the fitting parameters.

There was no discernable trend of frequency selectivity for any of the coupled hair bundles. We averaged the phase-locked amplitude of 8 bundles near the probe tip (<25μm) and 8 bundles farther away (between 25μm and 50μm). Both showed a linearly declining trend (Figure 13B, indicating that the coupled system acted mostly as a passive filter).

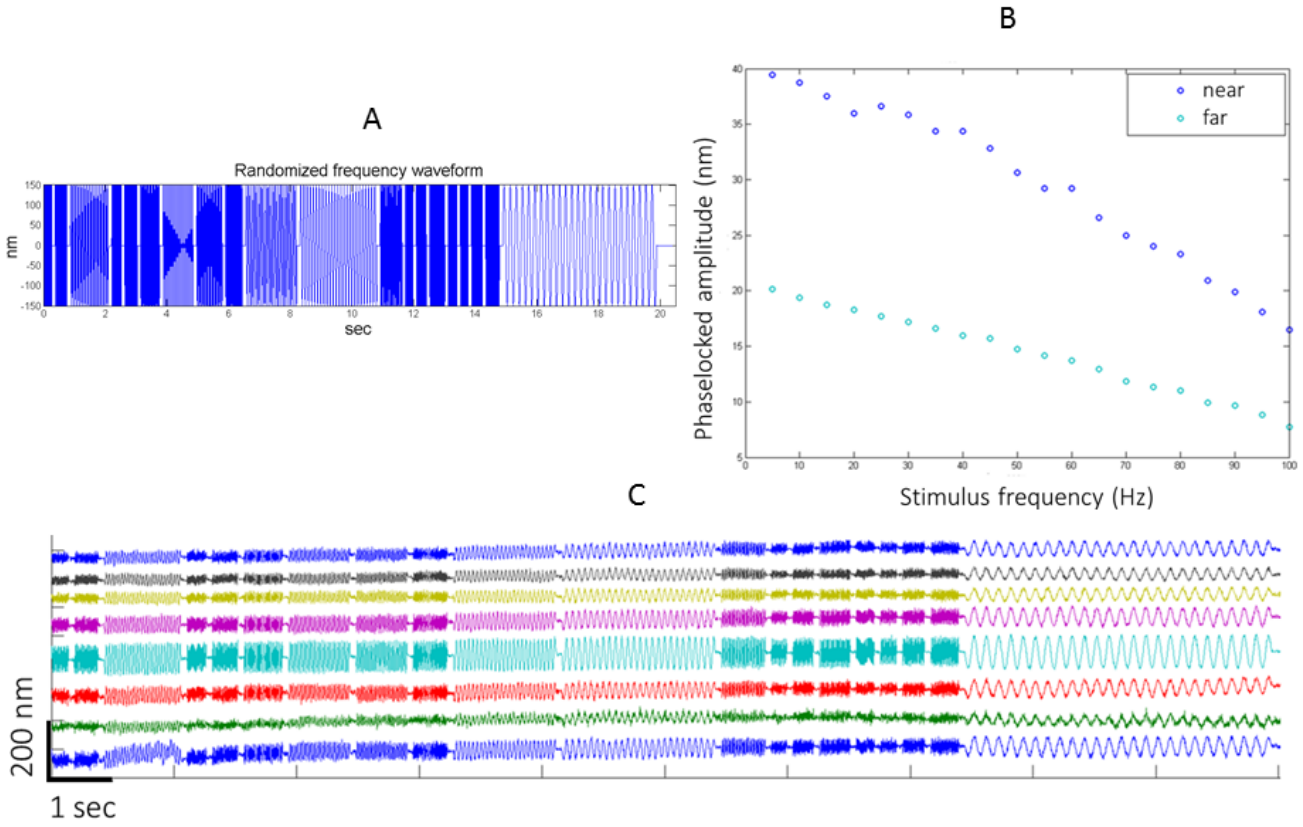

Figure 14. Test for frequency tuning.

(A) Stimulus waveform is a discrete frequency sweep, with randomized frequency segments. **(B)** Phaselocked amplitude versus stimulus amplitude, averaged for 8 bundles near the probe location, and 8 bundles farther away. **(C)** Trances of bundle response to stimulus, for 8 bundles near the probe location.

The result contrasts with the smaller coupled system, which showed a tuned response. Since the otolithic membrane couples many more bundles, with a much larger frequency dispersion, it is possible that the loss of tuning is due to dispersion. Further theoretical work is needed to demonstrate the size of the coupled ensemble at which the transition between tuned and not tuned response occurs.

4. Nonlinearity

We further examined whether the compressive nonlinearity, exhibited by individual bundles and small systems of coupled bundles, is retained in preparations in which few thousand bundles are coupled by the otolithic membrane. We applied a discrete amplitude sweep (Figure 15A), with sine waves at 33Hz, with 33 cycles per amplitude segment. The order of the applied amplitudes was randomized to prevent cumulative effects of adaptation, and the amplitude ranged from 10nm to 150nm.

Bundles within 50μm of the probe tip showed entrainment to the stimulus (Figure 15C). We measured the phase-locked amplitude in each discrete stimulus train, by fitting the response trace to a sine wave at the stimulus frequency. If there was any nonlinearity in the response, it would be observed in the phase-locked amplitude versus stimulus amplitude plot.

The result from our measurement was linear (Figure 15B), for both bundles near the probe tip and bundles farther away. This was a surprising result, and contrasted with our findings on the smaller coupled system, where coupled bundles exhibited compressive nonlinearity near resonance frequency. Since 33Hz is in the middle of hair bundle's frequency range, the stimulus was selected to be near the characteristic frequency of a significant fraction of the bundles. Nevertheless, no nonlinearity was ever observed.

Even though the amplitude trend looked linear, the active process in the coupled bundles could still have some effect on their mechanical response. To observe if there is indeed any effect, we stopped the active process by adding 50μM gentamicin to the endolymph solution. After allowing 3 minutes for the gentamicin to perfuse, we repeated the same stimulus on the otolithic membrane, and once again measured the phase-locked amplitude of the underlying hair bundles.

There was no measurable difference between hair bundle response with or without gentamicin (Figure 16). This indicated that the lack of nonlinear dynamics in this coupled occurred despite the presence of active process. The disappearance of nonlinearity could be due to coupling a dispersive array of oscillators, or it could be due to loading by the otolithic membrane.

We note that in the natural environment, the sacculus contains an additional mass load, consisting of the otoconia that lie atop the membrane. Future work would entail exploring the possible role of mass in restoring a nonlinear response of the coupled system.

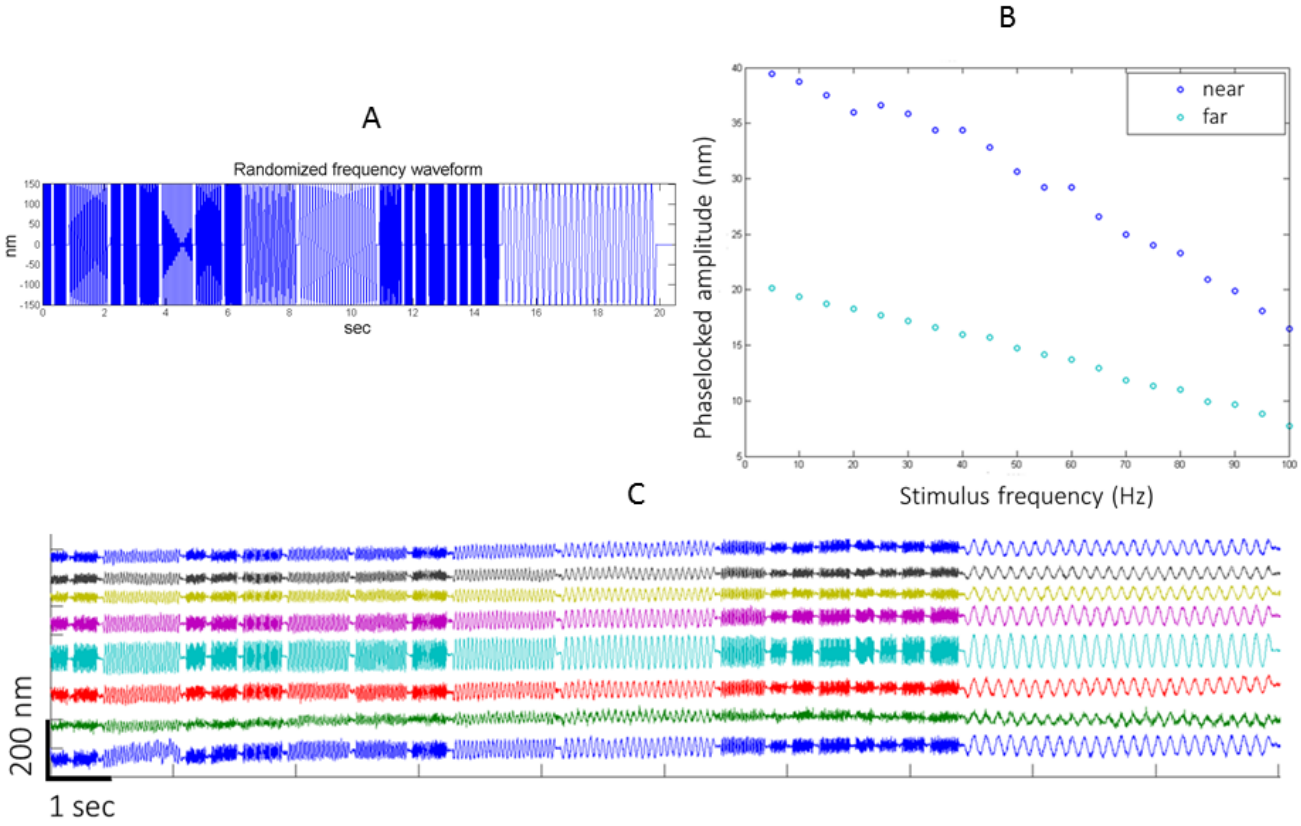

Figure 15. Test for nonlinearity.

(A) Discrete amplitude sweep stimulus waveform. Each segment is a sine wave stimulus at 33Hz, with 33cycles. **(B)** Phase-locked amplitude versus stimulus amplitude, for hair bundles near the probe tip (<25µm) and farther away (between 25µm and 50µm). **(C)** The response of 20 hair bundles to the stimulus, all of which located within 50µm of probe tip.

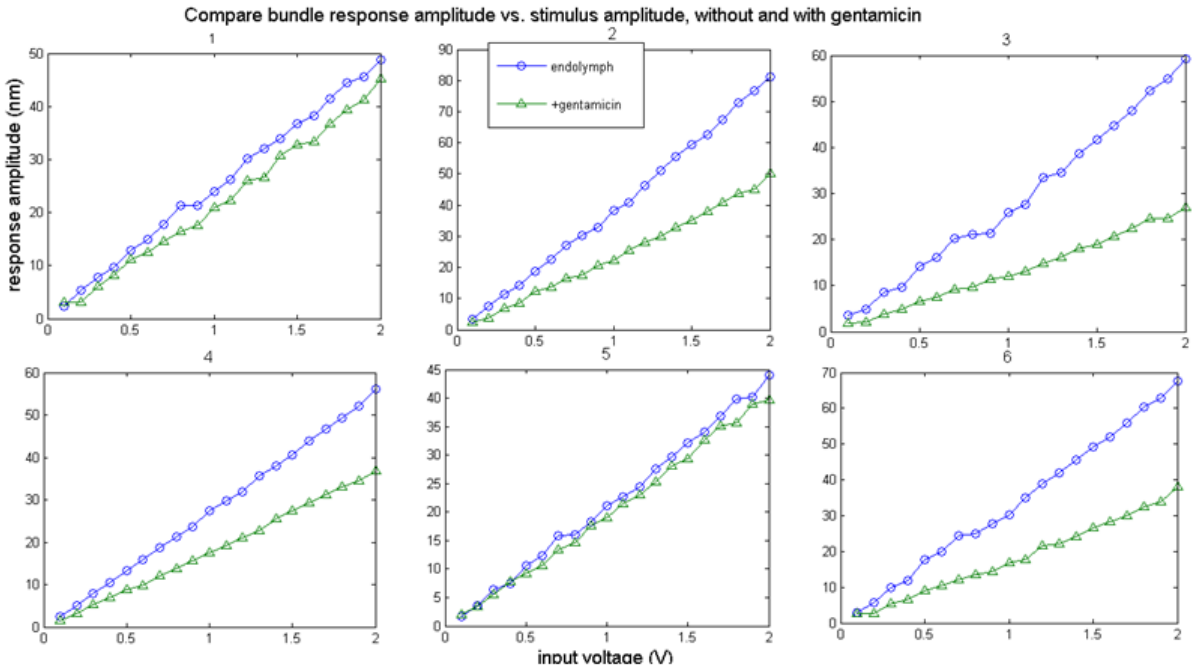

Figure 16. Comparison with control experiment.

Comparison between bundle response with and without gentamicin. Each panel shows the phase-locked amplitude versus stimulus frequency for one hair bundles, with the endolymph and gentamicin results overlaid.

Chapter 6. Chaos in a Coupled System

1.Motivation

The hair bundle exhibits spontaneous oscillation, which shows some periodicity, but is not entirely regular. The distribution of local periods has a spread, and empirical observations have shown that a bundle's oscillation profile can change over time. Prior work [19] has suggested that bundle oscillations are modulated by a time varying parameter. If this control parameter is also a dynamic variable, the system can exhibit quasiperiodic behavior [20]. In a particular parameter regime, a system described by three or more dynamic variables could become chaotic.

Demonstrating the level of chaos in the bundle dynamics would shed light on what modulating processes are at play. Prior work [21] has shown that an individual hair bundle oscillation is chaotic. A theoretical model furthermore showed that chaos might be correlated with the system's sensitivity to external stimuli [22]. According to the model, a bundle would exhibit higher sensitivity when weakly chaotic than in a purely deterministic limit-cycle regime. Since the coupled system had more degrees of freedom, we wanted to see how the level of chaos changes with coupling, and whether that change also leads to higher or lower sensitivity.

2. Poincare Map

Poincare map provides a qualitative measure of whether a system is deterministic or chaotic. For an oscillatory system, the map would plot the time interval between two events, against a previous time interval. If the system has one frequency and is completely regular, the map would consist of a point. If the oscillations are modulated by another oscillating process

(quasiperiodic), then the map would show a ring. The quasi-periodic transition is one of the well known routes to chaos. When the system reaches the chaotic regime, it exhibits a cloud.

Figure 17 shows the result from one set of coupled bundles. The intervals I_n are the cycle periods. There were four bundles in this group, where bundle 1-3 were synchronized one-to-one under the bead, and bundle 4 was multimode-locked. The Poincare map under coupled and de-coupled conditions are overlaid together. Under both conditions, the map shows a cloud of points, which is consistent with the oscillations being chaotic. We note however, that stochastic noise likewise leads to scatter, and that additional tests of chaos need to be performed. Though some groups of bundles exhibited slightly smaller clouds under coupled than de-coupled conditions, we could not make a definitive comparison.

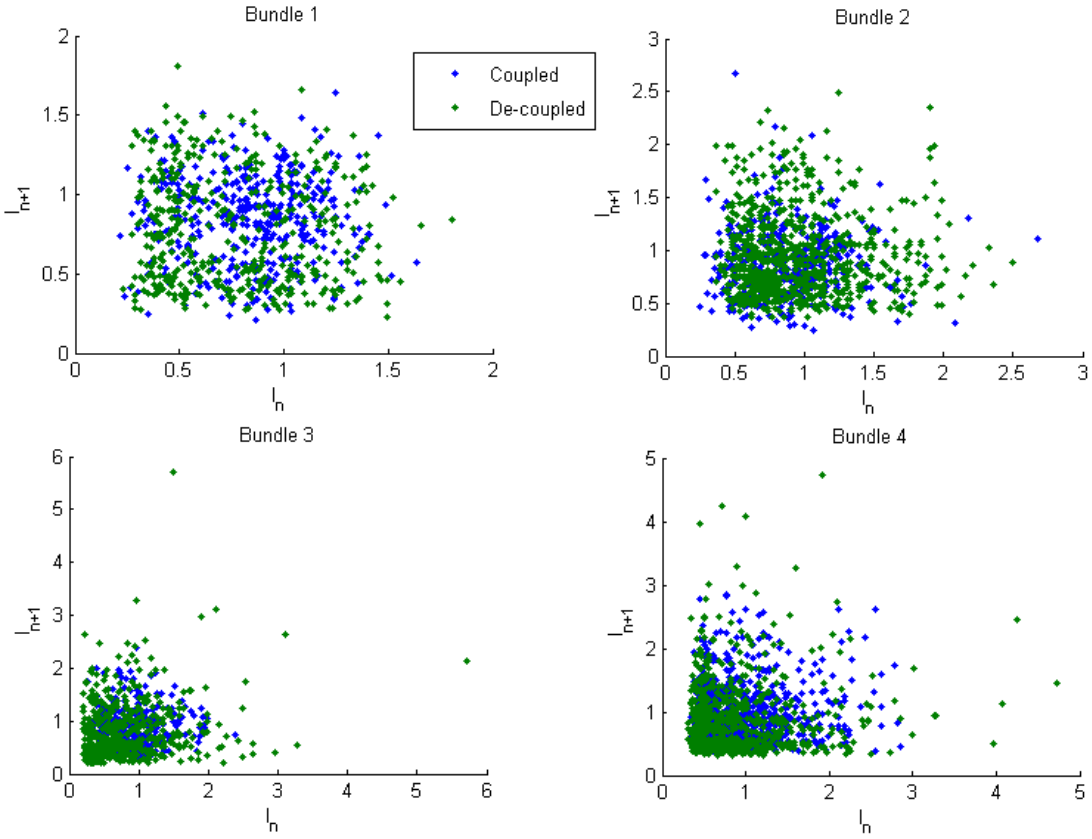

Figure 17. Poincare map of bundle trajectories.

Poincare map for coupled and de-coupled bundles. Each subplot shows a single bundle in the same group, under both coupled and de-coupled conditions. I_n are the intervals (periods) of oscillations, normalized by multiplication with the characteristic frequency. I_{n+1} are the previous periods.

3. Quasiperiodic transition

Poincare maps of spontaneous oscillations could not be used to distinguish chaos from noise. To mitigate this problem, we imposed a mechanical stimulus to the coupled system. The stimulus imposed was a sine wave with ramped amplitude, applied at the resonance frequency of the group of hair bundles (Figure 18A). Over one minute, the stimulus amplitude increased from 0nm to 90nm. We examined three time windows representing the early, middle, and late

stimulus stages (Figure 18 B-D). Each window was 10 seconds long, and the mean stimulus amplitude in the window was 7.5nm, 45nm, and 82.5nm, respectively.

The Poincare map in these time windows gave clue to the evolution of the bundle's dynamical state. When stimulus was small, the Poincare map showed a ring structure (Figure 18B), which is one of the hallmarks of quasiperiodicity. This transition occurred when the bundle's oscillation was modulated by a periodic drive (the stimulus). As stimulus grew stronger, bundles became more entrained, and the quasiperiodic behavior disappeared. Consequently, the ring in the Poincare map collapsed into clusters (Figure 18C). In late stage of stimulus, bundles became completely entrained, and the Poincare map was reduced to small clusters (Figure 18D). Due to the presence of the multimode-locked bundle, there was more than one cluster. Even after bundles had become completely entrained to the stimulus (at 5Hz), the influence of the multimode bundle (at 18Hz) was still apparent.

Quasiperiodic route to chaos is characterized by a phenomenon known as torus breakdown. This effect could be observed by testing the invertibility of the angle map [21]. The angle map was obtained by selecting an arbitrary origin in the Poincare map, and then measuring the angle of every point on the trajectory, with respect to the x axis. The resulting map from the early stage of stimulus is shown in Figure 19. Since the map was not invertible, this indicated that the quasiperiodic transition was chaotic.

In some of the cases tested, the quasiperiodic behavior was observed to persist up to very high stimulus amplitude. An example is shown in Figure 20D, where the ring structure in bundle 3 remained even after complete entrainment. This indicated that coupled systems had a broader range of complex dynamics than that of a single bundle.

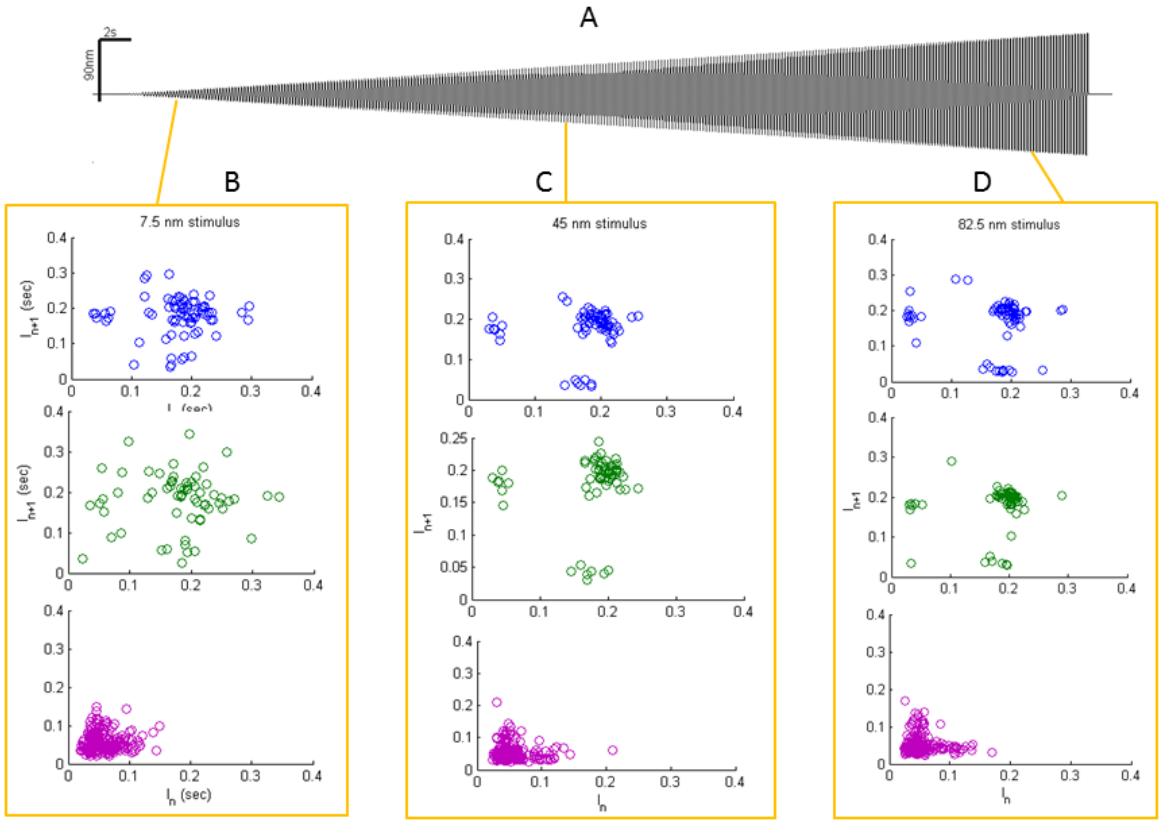

Figure 18. Quasiperiodic transition of bundle trajectories.

(A) Stimulus waveform consisting of sine wave at 5Hz, with amplitude increasing from 0nm to 90nm over one minute. **(B)**-**(D)** are select time windows that represent early, middle, and late stages of stimulus. Window size = 10 seconds, and mean stimulus in window = 7.5nm, 45nm, and 82.5nm, respectively. Each colored scatter plot is the Poincare map of one synchronized bundle.

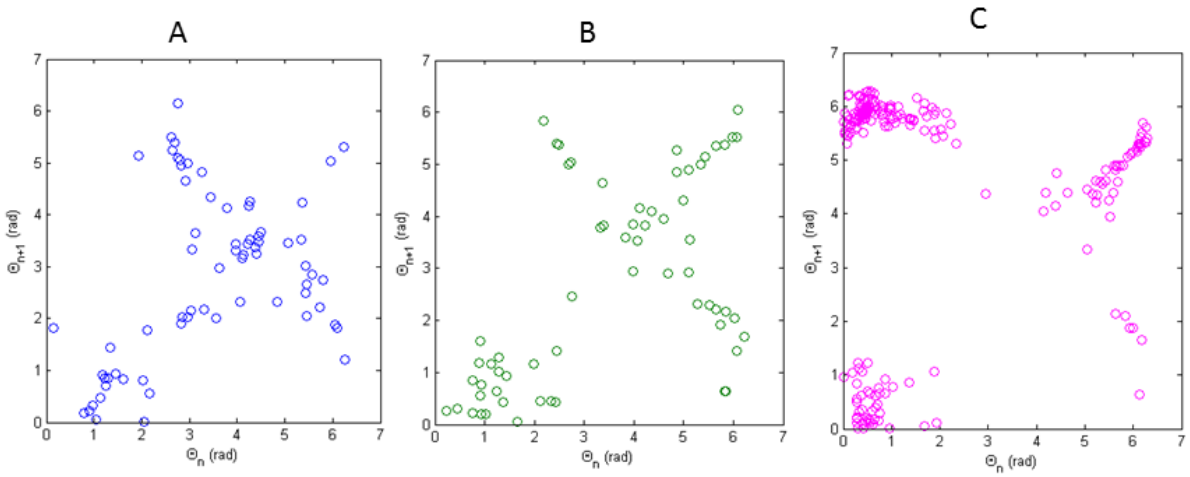

Figure 19. Angle map from the early stage of stimulus.
(A)-(C) Each panel is the angle map of one synchronized bundle, derived from panel (A) in Figure 19. Θ was measured from an arbitrarily chosen origin and x-axis in the original Poincare map.

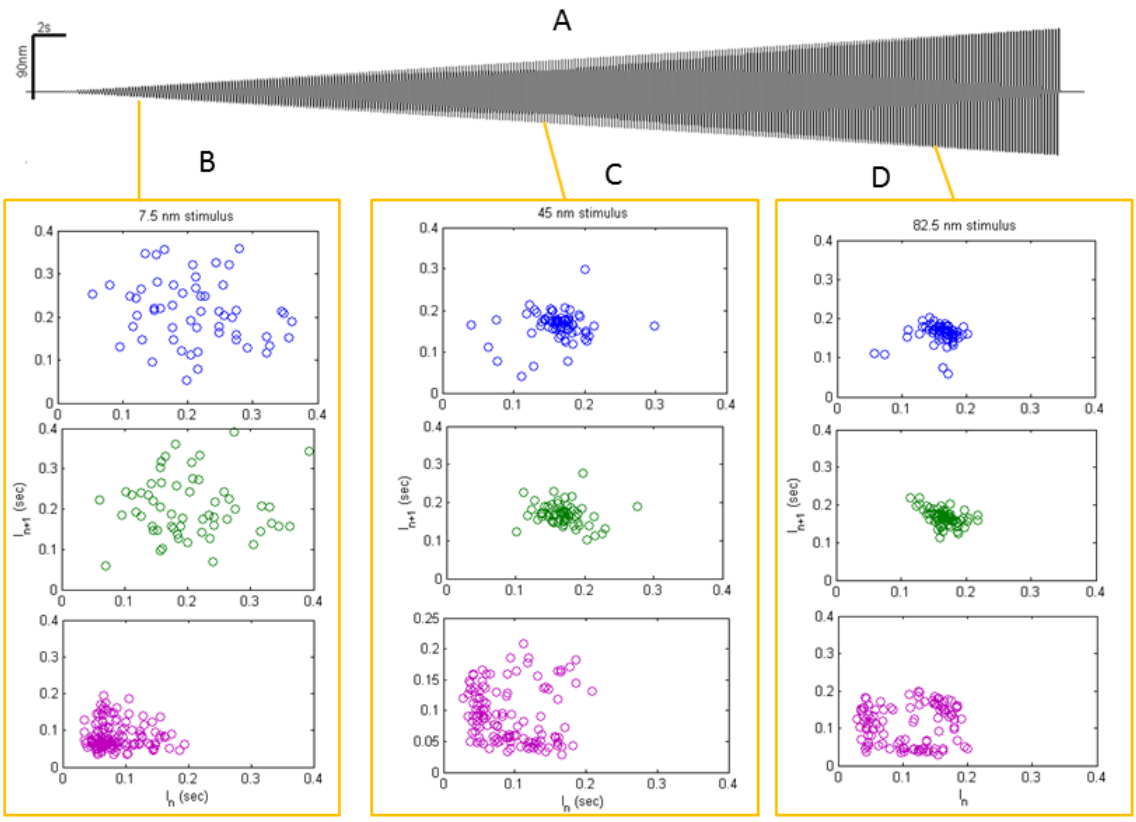

Figure 20. Quasiperiodic transition, case II.

(A) Stimulus waveform consisting of sine wave at 6Hz, with amplitude increasing from 0nm to 90nm over one minute. **(B)**-**(D)** are select time windows that represent early, middle, and late stages of stimulus. Window size = 10 seconds, and mean stimulus in window = 7.5nm, 45nm, and 82.5nm, respectively. Each colored scatter plot is the Poincare map of one synchronized bundle.

3. Kolmogorov Entropy

Poincare map provided a qualitative measurement of chaos. For a quantitative measurement, we used the Kolmogorov entropy method.

For this method, we first needed to reconstruct a higher dimensional phase space. The measured oscillation trace x(t) was a one-dimensional time series. We used a procedure described in [20] to reconstruct the higher dimensional phase space that the trajectory occupied.

We picked a time shift parameter, τ, and mapped x(t) onto x(t+τ), x(t+2τ), x(t+3τ), and x(t+4τ) (Figure 21A). Thus, every point in x(t) is mapped onto a point in 5-dimensional space, with coordinates given by [x(t), x(t+τ), x(t+2τ), x(t+3τ), x(t+4τ)].

The time shift parameter τ was chosen so that the projections onto each dimension would have minimal correlation with each other. This was determined from the autocorrelation function of x(t), where τ was defined as the first zero crossing of the autocorrelation function [Figure 21B].

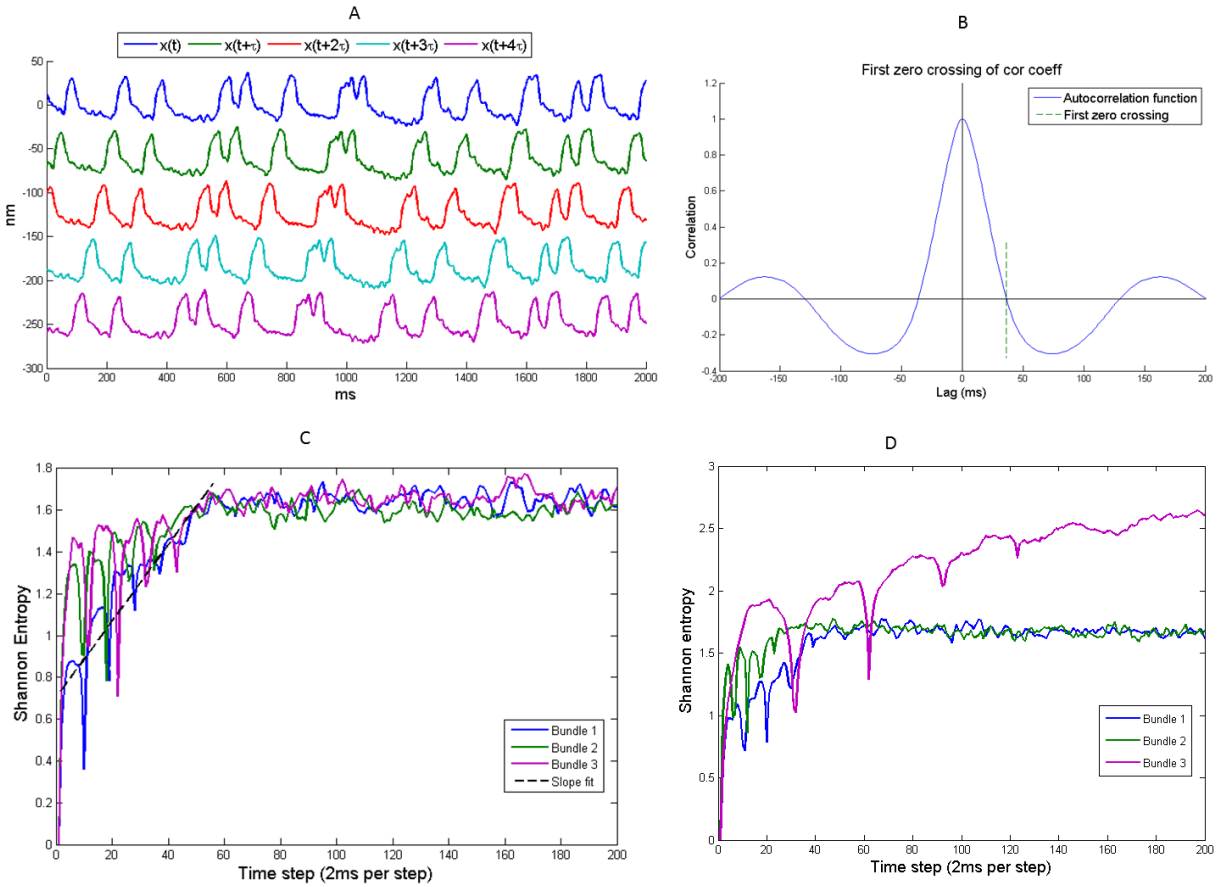

Figure 21. The Shannon entropy of bundle trajectories.

(A) Phase space reconstruction by time shift. The oscillation trace x(t) is shifted by τ, 2τ, 3τ, and 4τ. Each point in x(t) is thus mapped onto a point in 5-dimensional space, with coordinates given

by [x(t), x(t+τ), x(t+2τ), x(t+3τ), x(t+4τ)]. **(B)** Autocorrelation function of x(t). The location of the first zero crossing is chosen to be the time shift parameter τ. **(C)** The time evolution of Shannon entropy for a synchronized group. Each colored line represents S_n for one synchronized bundle. The dashed line represents the linear fit of the initial increase. The slope of the fit gives the Kolmogorov entropy. **(D)** Shannon entropy for the same group of bundles as in (C), while they oscillated freely. Each colored line represents a de-coupled bundle.

In the reconstructed phase space, we could track the time evolution of the bundle's trajectory. We divided the phase space into 5-dimensional hypercubes, and tracked the trajectory of points starting from one hypercube. As time progressed, the points would spread over other hypercubes. The rate of this growth can be measured by Kolmogorov entropy. The Kolmogorov entropy is defined as

$$K = \lim_{T\to 0}\lim_{\varepsilon\to 0}\lim_{N\to\infty}\frac{1}{NT}\sum_{n=0}^{N-1} S_{n+1} - S_n$$

where ε refers to the size of the hypercube (each box has side length ε on each dimension), T refers to the time step, and S_n refers to the Shannon entropy, which is defined as

$$S_n = -\sum_{p_i} Prob_{p_i}\ln(Prob_{p_i})$$

The sum is computed over a particular path of hypercubes, referred to as P_i. The path consists of a trajectory through n hypercubes. Hence, the trajectory would have to be in the 1st hypercube at time t=0, in the 2nd hypercube at time t = T, and in the nth hypercube at time t+(n-1)*T. The probabilities in the sum are associated with this trajectory. Since the choice of the path is arbitrary, we also want to average many different paths to obtain the best estimate of the Shannon entropy.

Although we couldn't observe the limits T→0 and N→∞, we found that T = 2ms and N = 200 steps were sufficient for asymptotic trends to emerge in the Shannon entropy. Moreover, we

found that too finely divided hypercubes (very small ε) led to very sparse point distribution, making computations inefficient. Therefore, we divided the phase space empirically so that many of the hypercubes were well-occupied (containing 50 points or more). This corresponded to 4 divisions per dimension, or 4^5 hypercubes in total. We also randomly chose 50 paths, and averaged the Shannon entropy value over these paths.

We examined the time evolution of Shannon entropy in order to determine Kolmogorov entropy. Figure 21C shows data from one synchronized group, plotting each bundle's Shannon entropy change over time. Figure 21D shows the Shannon entropy of these bundles when they were oscillating freely. Typically, S_n increased with time for approximately 150ms, before reaching a plateau. After plateauing, further slight changes in S_n likely reflected the measurement noise in the experimental recordings. The slope of the initial increase of S_n gave an estimate of the Kolmogorov entropy, which we determined by fitting a line (Figure 21C).

We compared K-entropy obtained this way for synchronized versus de-coupled bundles. The results reflected a complex effect. Within the same group of bundles, K-entropy was higher for some bundles while coupled, but lower for others. We speculate that details of the coupling conditions likely impacted the degrees of freedom exhibited by the system, and hence the chaoticity of the dynamics exhibited by the bundles.

Chapter 7. Other Coupling Techniques

1. Melted PLGA microsphere

1.1 Protocol

Melting the microsphere into a flat shape held the advantage that more of the hair bundles could be coupled, and it would allow for variation in the strength of coupling, by using different sizes of the artificial structures.

For starting material, we used microspheres made of Poly(lactide-co-glycolide), or PLGA, which is a biodegradable polymer. The thermal property of PLGA depends on the lactide:glycolide ratio. The variety we used had 25% glycolide, with a melting point of 170°C. Flat films measuring 50μm across were obtained from 30μm microspheres; 80μm films could be obtained from 50μm spheres.

To melt the microspheres, we first mixed it in deionized water at a concentration of 2mg/ml. Thin Teflon strips measuring 0.5cmX2cmX1mm were set on a hotplate, and the hotplate itself was positioned under a dissection microscope to enable visual confirmation of melting. Droplets of microsphere-water mixture were deposited onto the Teflon strips with a pipette. As water evaporated, the microspheres melted onto the Teflon strips. The melted films were detached from the Teflon strip with a scalpel. Next, a single Teflon strip was set vertically in a 1ml Eppendorf tube, with deionized water filling the tube. We sonicated the tube for 2 minutes, and discarded the Teflon, leaving the melted spheres in the tube.

The melted spheres were also coated with Concanavalin A and deposited onto the bundles with a pipette. They bound to bundles effectively, with less degree of freedom in the coupling. They were also less easily displaced by mechanical stimulus, allowing stimulus to reach greater

amplitudes. Moreover, the variability in size, depending on starting size of the round sphere, made it possible to couple more than 4 bundles.

1.2 Effectiveness

Melting 30μm sized PLGA spheres produced roughly 45μm films (Figure 23A). They could also couple 2-4 bundles, similar to the 50μm polystyrene beads.

Melting 50μm sized PLGA spheres produced larger films, roughly 80μm in diameters. They could cover as many as 20 bundles underneath, though not all of them would be synchronized. We observed one case of 4 bundles synchronized one-to-one, with two more exhibiting multimode synchronization (Figure 23B). Hence, for melted polylactide beads constitute an effective potential way to scale up the coupled system in future studies.

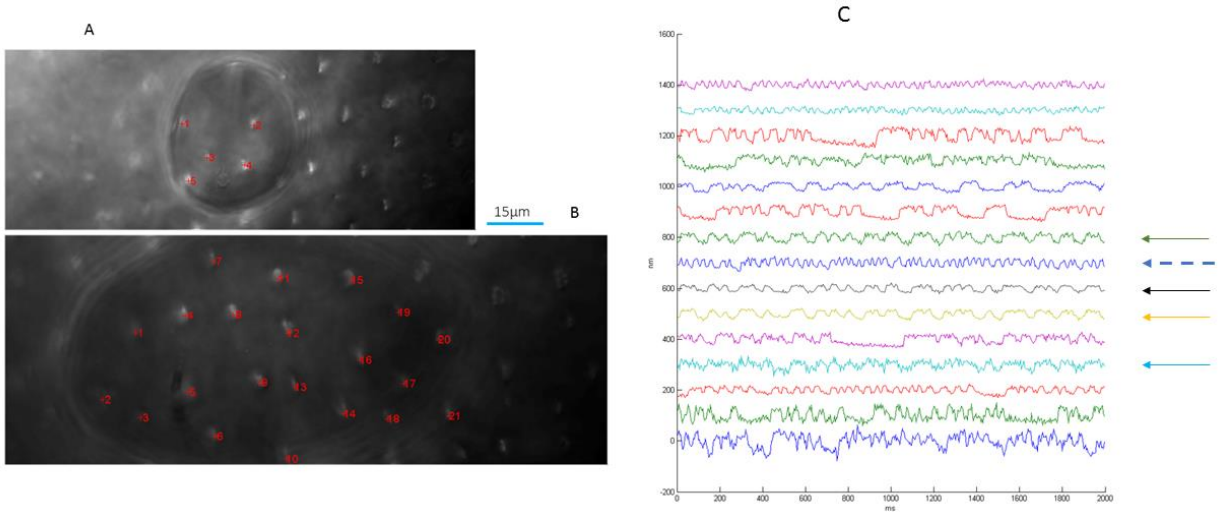

Figure 22. Melted PLGA beads.

(A) A 45μm-sized film, resulting from melting a 30μm bead. **(B)** A 80μm-sized film, resulting from melting a 50μm bead. **(C)** Bundles coupled by the 80μm film. Each colored trace represents one bundles. Solid arrows indicate those synchronized one-to-one, while dashed arrows indicate the multimode-locked bundles.

2. Novel glass probes

Glass probes with low stiffness (<200μN/m) could also be used to couple hair bundles, without suppressing the innate oscillations. The biggest advantage in using glass probes was the ability to target specific hair bundles, as the probe was mounted on a movable plate. This section describes several glass probe shapes tested for future applications.

A. Twice-bent probes. These probes were bent with a microforge at such angles so that the tip section was horizontal. They could thus be lowered onto the preparation, and attached to two bundles simultaneously. They thus provided a very effective means of coupling two bundles; the method however could not be readily scaled up.

B. Spiral probes. These probes were bent so that the tip produced a horizontal spiral. The tip could be attached on the top of bundles, and couple bundles in a circle. The advantage of the approach in that it could yield a number of connected bundles. Attachment to the bundles was difficult to control, however, and visibility through the probe was poor.

C. Microsphere melted onto a probe. During the procedure used to melt PLGA microspheres, a probe with a horizontal end could be lowered onto the Teflon strip and pushed against a melting microsphere. The probe tip would be embedded into the melted film, and be able to lift the film off the Teflon strip after the heat was reduced. The probe-film configuration was stable, and could be used as a coupling agent. The advantage of the technique is that would allow placing the melted bead onto selected bundles, with a probe already attached. The biggest drawback, however, was the probe stiffness. In order to hold the melted film at a set angle, the probe had to be sufficiently stiff, too stiff to couple bundles without suppressing oscillations.

The techniques explored all had advantages and drawbacks, and could be explored in future studies of coupling effects on hair bundle dynamics.

Chapter 8. Conclusion

1. Spontaneous motility

Our results demonstrate synchronization between spontaneously oscillating hair cell bundles of the inner ear. These experiments confirm theoretical predictions for synchronization under coupled conditions [8], in a biological preparation that maintains the functional integrity of the hair cells. Coherent active motility of the bundles was clearly sufficient to drive the oscillations of the overlying bead in a viscous fluid environment. Synchronization was observed in the systems studied, despite significant dispersion of the characteristic frequencies of the constituent oscillators.

Hair bundles oscillated more regularly when coupled to the overlying bead. The quality factors of the coupled bundles were ~1.2–1.8x larger than those of the individual bundles. Slightly higher enhancement (2x) was observed in the system where one hair bundle was coupled to its cyber clone [9]. The theoretical model for a coupled system of 2x2 identical oscillators showed a 4-5x increase in the quality factor under conditions of strong coupling [8]. The enhancement was therefore higher than what was observed in our hybrid preparations.

We ascribe the discrepancy to the frequency dispersion of the biological system. In both of the prior studies, the coupled bundles were chosen to exhibit identical innate frequencies, whereas the saccular epithelium displays broad frequency dispersion. The enhancement of the quality factor, present despite dispersion in the frequencies of constituent oscillators, indicates the importance of coupling in shaping the frequency tuning of the whole system.

2. Driven response

Synchronized hair bundles displayed frequency tuning, which was similar to the behavior of individual hair bundles [14]. Although theory predicted enhanced frequency tuning [8], the tuning curved we observed was broad, encompassing the natural frequencies of all bundles synchronized. This effect is likely also due to the dispersion of innate frequencies observed in saccular hair bundles.

We also observed compressive nonlinearity in synchronized hair bundles. This behavior was similar to individual hair bundles [7], where the response was nonlinear for stimulus near resonance, and less so off-resonance. Despite the presence of innate frequency dispersion, which complicated the picture of resonance frequency, compressive nonlinearity was retained. The shape of the power-law for on-resonance frequency was also similar to the value obtained in individual hair bundles [7].

We also explored quasiperiodic behavior in the driven response. Synchronized hair bundles typically displayed quasiperiodicity at low stimulus amplitudes, where entrainment was low. This was similar to single bundles [21]. We also demonstrated that chaos could arise from these quasiperiodic transitions. However, unlike single bundles, synchronized bundles could sustain quasiperiodic behavior even with very high entrainment. Moreover, multiple clusters could be present in the bundle's Poincare map, indicating the influence of multi-mode synchronization between bundles. Since chaos could have beneficial effect on mechanical sensitivity [22], our results indicate another potential relationship between coupling and sensitivity.

3. Different scales of coupled systems

Comparing the driven response in the small coupled system (bead) and the large array (with otolithic membrane), we observed significant differences. The large system did not show any indication of frequency tuning. Moreover, its mechanical response appeared to be completely linear. Loading by the otolithic membrane, as well as the very broad frequency dispersion in the large array of cells, likely account for these phenomena. Concurrent theoretical work is exploring numerical models of the data. Future work could shed more like on the intermediate regime between the small and large system.

Our findings indicate that coupling between hair bundles leads to a rich array of phenomena, affecting the sensitivity, nonlinearity, frequency selectivity, and dynamics of the system. As auditory and vestibular systems in nature exhibit various degrees of coupling, understanding its effects on detection is an important step in accounting for this rich diversity of structures.

References

[1] A. J. Hudspeth, "Hearing," in *Principles of Neural Science*, New York, McGraw-Hill, 2000, pp. 590-624.

[2] P. G. Gillespie and U. Muller, "Mechanotransduction by hair cells: models, modecules, and mechanisms," *Cell,* vol. 139, no. 1, pp. 33-44, 2009.

[3] T. Gold, "Hearing II. The physical basis of the action of the cochlea," *Proceedings of the Royal Society of London B,* vol. 135, p. 492, 1948.

[4] Hudspeth, "Integrating the active process of hair cells with cochlear function," *Nature Review Neuroscience,* vol. 15, pp. 600-614, 2014.

[5] P. Martin, D. Bozovic, Y. Choe and A. J. Hudspeth, "Spontaneous oscillation by hair bundles of the bullfrog's sacculus," *Journal of Neuroscience,* vol. 23, no. 11, pp. 4533-4548, 2003.

[6] M. LeMasurier and P. G. Gillespie, "Hair-cell mechanotransduction and cochlear amplification," *Neuron,* vol. 48, no. 3, pp. 403-415, 2005.

[7] P. Martin and A. J. Hudspeth, "Compressive nonlinearity in the hair bundle's active response to mechanical stimulation," *Proceedings of the National Academy of Sciences of the United States of America,* vol. 98, no. 25, pp. 14386-14391, 2001.

[8] K. Dierkes, B. Lindner and F. Julicher, "Enhancement of sensitivity gain and frequency tuning by coupling of active hair bundles," *Proceedings of the National Academy of Sciences of the United States of America,* vol. 105, no. 48, pp. 18669-18674, 2008.

[9] J. Barral, K. Dierkes, B. Lindner, F. Julicher and P. Martin, "Coupling sensory hair-cell bundles to cyber clones enhances nonlinear amplification," *Proceedings of the National Academy of Sciences of the United States of America,* vol. 107, no. 23, p. 10765, 2010.

[10] K. H. Ahn, "Enhanced signal-to-noise ratios in frog hearing can be achieved through amplitude death," *Journal of Royal Society Interface,* no. 10, pp. 525-533, 2013.

[11] C. E. Strimbu, A. Kao, J. Tokuda, D. Ramuno-Johnson and D. Bozovic, "Dynamic state and evoked motility in coupled hair bundles of the bullfrog sacculus," *Hearing Research,* vol. 265, no. 12, pp. 38-45, 2010.

[12] M. S. Smotherman and P. M. Narins, "Hair cells, hearing and hopping: a field guide to hair cell physiology in the frog," *The Journal of Experimental Biology,* no. 203, p. 2237–46, 2000.

[13] D. Ramunno-Johnson, C. E. Strimbu, L. Fredrickson-Hemsing, K. Arisaka and D. Bozovic, "Distribution of frequencies of spontaneous oscillations in hair cells of the bullfrog sacculus," *Biophysical Journal,* vol. 96, no. 1159, 2009.

[14] L. Fredrickson-Hemsing, S. Ji, R. Bruinsma and D. Bozovic, "Mode-locked dynamics of hair cells of the inner ear," *Physical Review E,* vol. 86, no. 2, 2012.

[15] P. Martin and A. J. Hudspeth, "Active hair-bundle movements can amplify a hair cell's response to oscillatory mechanical stimuli," *Proceedings of the National Academy of Sciences of the United States of America,* vol. 96, no. 25, p. 14306–14311, 1999.

[16] D. E. Hillman and E. R. Lewis, "Morphological basis for a mechanical linkage in otolithic receptor transduction in the frog".

[17] M. E. Benser, N. P. Issa and A. J. Hudspeth, "Hair-bundle stifiness dominates the elastic reactance to otolithic-membrane shear," *Hearing Research,* vol. 68, pp. 243-252, 1993.

[18] C. E. Striumbu, L. Fredrickson-Hemsing and D. Bozovic, "Coupling and Elastic Loading Affect the Active Response by the Inner Ear Hair Cell Bundles," *Plos One,* 2012.

[19] R. Shlomovitz, L. Fredrickson-Hemsing, A. Kao, S. W. F. Meenderink, R. Bruinsma and D. Bozovic, "Low Frequency Entrainment of Oscillatory Bursts in Hair Cells," *Biophysical Journal,* vol. 104, no. 8, pp. 1661-1669, 2013.

[20] A. Garfinkel, P. S. Chen, D. O. Walter, H. S. Karagueuzian, B. Kogan, S. J. Evans, M. Karpoukhin, C. Hwang, T. Uchida, M. Gotoh, O. Nwasokwa, P. Sager and J. N. Weiss, "Quasiperiodicity and chaos in cardiac fibrillation," *Journal of Clinical Investigation,* vol. 99, no. 2, pp. 305-314, 1997.

[21] J. Faber and D. Bozovic, "Chaotic Dynamics of Inner Ear Hair Cells," *Arxiv,* p. 1702.02703.

[22] A. B. Neiman, K. Dierkes, B. Lindner, L. Han and A. L. Shilnikov, "Spontaneous voltage oscillations and response dynamics of a Hodgkin-Huxley type model of sensory hair cells," *Journal of Mathematical Neuroscience,* vol. 1, no. 11, 2011.

[23] A. J. Hudspeth, "Making an effort to listen: mechanical amplification in the ear," *Neuron,* vol. 59, no. 4, pp. 530-545, 2008.